WSRC-TR-2002-00548
SRT-RPP-2002-00272

Determination of Perrhenate (ReO_4^-) Adsorption Kinetics from Hanford Waste Simulants using SuperLig® 639 Resin (U)

Westinghouse Savannah River Company
Savannah River Site
Aiken, SC 29808

Prepared for the U.S. Department of Energy under Contract No. DE-AC09-96SR18500

WSRC-TR-2002-00548
SRT-RPP-2002-00272

KEYWORDS:
Hanford River Protection Project
Ion-exchange
Kinetics
Rhenium
Perrhenate
Technetium
SuperLig® Resins
RETENTION - Permanent

Determination of Perrhenate (ReO_4^-) Adsorption Kinetics from Hanford Waste Simulants using SuperLig® 639 Resin (U)

SAVANNAH RIVER TECHNOLOGY CENTER

Cheryl E. Duffey
William D. King
L. Larry Hamm

Publication Date: April 2003

Westinghouse Savannah River Company
Savannah River Site
Aiken, SC 29808

Prepared for the U.S. Department of Energy under Contract No. DE-AC09-96SR18500

SAFETY • RESPONSIBILITY • SECURITY
SRS
SAVANNAH RIVER SITE

DOCUMENT: **WSRC-TR-2002-00548 (SRT-RPP-2002-00272)**
TITLE: **Determination of Perrhenate (ReO_4) Adsorption Kinetics from Hanford Waste simulants using SuperLing® 639 Resin**

APPROVALS:

_____ Date_____
Cheryl E. Duffey, Co-Author/SRTC/Waste Processing Technology

_____ Date_____
William D. King, Co-Author/SRTC/Waste Processing Technology

_____ Date_____
L. Larry Hamm, Co-Author/SRTC/EngineeringDevelopment

_____ Date_____
James C. Marra/SRTC/Waste Processing Technology/Level 4 Manger

_____ Date_____
Sebastian Aleman/SRTC/Technical Reviewer

_____ Date_____
Reid Peterson/Bechtel/River Protection Project

TABLE OF CONTENTS

LIST OF TABLES

LIST OF FIGURES

(This Page Intentionally Left Blank)

TABLE OF NOTATION

$\overline{C}_T$	Total perrhenate adsorption capacity, mmol of ReO_4/gram of dry resin
c_f	Liquid-phase rhenium concentration at equilibrium (final conc.), [M]
$c_f(t)$	ReO_4 liquid-phase concentration at time t, [M]
c_f^{min}	Minimum measured ReO_4 liquid-phase concentration during test, [M]
c_i	Initial ReO_4 liquid-phase concentration, [M]
$\Delta c(t)$	Reduction in liquid-phase ReO_4 concentration at time t, [M]
D_{pi}	Species i pore diffusion coefficient, cm^2/min
$D_{\infty i}$	Species i free-stream diffusion coefficient, cm^2/min
F	F-factor for conversion from filter-dried to oven-dried resin mass, (-)
[i]	Liquid- or solid-phase concentrations of compound i, M or mmol/L (respectively)
k_f	Film diffusion coefficient, cm/min
$K_{eq,i}(T)$	Thermodynamic equilibrium constant for mass action equation i, $[M^{-1}]$
$\tilde{K}_{21}$	Selectivity coefficient for perrhenate versus nitrate competition, (-)
K_d	Chord of isotherm at a equilibrium liquid-phase ReO_4 concentration level
$K_d(t)$	Distribution coefficient at time t, ml/g
L	Ligand adsorption sites, (-)
m_d	Mass of oven-dried resin, g
m_i	Mass of filter-dried resin, g
Q	Perrhenate loading on resin, mmol of Re/gram of dry resin
T	Liquid-phase temperature (contact temperature), ºC
u_o	Superficial velocity through bed, cm/min
V_{soln}	Volume of liquid-phase sample, ml
<	Minimum detection limit (tables listing specie concentrations)

Greek

β	Beta parameter reflecting impact of nitrate competitor, [M]
$\eta(t)$	Normalized liquid-phase ReO_4 concentration at time t, (-)
γ_i	Liquid-phase activity coefficient for species i, (-)
ϕ	Phase ratio (liquid-to-resin), ml of solution/gram of dry resin
τ	Tortuosity factor for pores within SuperLig® 639 particles, (-)

1.0 Executive Summary

This report describes the results of SuperLig® 639 sorption kinetics tests conducted at the Savannah River Technology Center (SRTC) in support of the Hanford River Protection Project - Waste Treatment Plant (RPP-WTP). The RPP-WTP contract was awarded to Bechtel for the design, construction, and initial operation of a plant for the treatment and vitrification of millions of gallons of radioactive waste currently stored in tanks at Hanford, WA. Part of the current treatment process involves the removal of technetium from tank supernate solutions using columns containing SuperLig® 639 resin. This report is part of a body of work intended to quantify and optimize the operation of the technetium removal columns with regard to various parameters (such as liquid flow rate, column aspect ratio, resin particle size, loading and elution temperature, etc.). The tests were conducted using nonradioactive simulants of the actual tank waste samples containing rhenium as a chemical surrogate for the technetium in the actual waste. Previous column tests evaluated the impacts of liquid flow rate, bed aspect ratio, solution temperature and composition upon SuperLig® 639 column performance (King et al., 2000, King et al., 2003). This report describes the results of kinetics tests to determine the impacts of resin particle size, solution composition, and temperature on the rate of uptake of perrhenate ions.

1.1 Objectives

Primary test objectives included:

- Develop a test apparatus for the accurate measurement of perrhenate sorption kinetics with SuperLig® 639 resin and Hanford waste simulants;
- Identify a test method to resolve contributions of pore and film diffusion processes to the overall rate of perrhenate uptake by SuperLig® 639 resin ;
- Determine the impacts of temperature and resin particle size on rhenium sorption kinetics with SuperLig® 639 resin and Hanford Tank 241-AN-105 (Envelope A) waste simulant; and
- Determine the impact of solution composition on rhenium sorption kinetics with SuperLig® 639 resin and waste simulants of Hanford Tanks 241-AN-105 (Envelope A), 241-AZ-102 (Envelope B), and 241-AN-107 (Envelope C).

1.2 Conduct of Testing

Tests were performed with SuperLig® 639 resin using three Hanford waste simulants. Perrhenate ion was utilized as a surrogate for pertechnetate ion so that the tests could be performed in a nonradiological fume hood at minimal cost. All kinetics testing was performed using the kinetics test apparatus described herein and approximately 1.3 mL of filter-dried SuperLig® 639 resin. Temperature dependent kinetics tests were performed using unsieved resin, AN-105 simulant, a flow rate of 30 mL/min (12.5 cm/min), and experimental temperatures of 25, 35, and 45°C. To confirm reproducibility of the kinetics test apparatus and methodology, the test at 25°C was repeated. This test was considered to be under nominal conditions and was

used in all comparisons. Particle size dependent kinetics tests were performed using AN-105 simulant at 25°C, a flow rate of 30 mL/min (12.5 cm/min), and resin sieve fractions of 10-20 mesh, 20-40 mesh, and 40-60 mesh. Flow rate dependent kinetics tests (for resolution of pore and film diffusion contributions) were conducted using unsieved resin, AN-105 simulant at 25°C, and flow rates of 1 mL/min (0.416 cm/min) and 0.5 mL/min (0.208 cm/min).

Additional tests were performed at 25°C using unsieved resin, a flow rate of 30 mL/min (12.5 cm/min) and AZ-102 and AN-107 simulants. These experiments were also performed using the kinetics test apparatus and approximately 1.3 mL of filter-dried SuperLig® 639.

1.3 Results and Performance Against Objectives

Large variability has been observed and reported by Hamm et al. (2000a and 2000b) in the existing K_d databases (which consist of complied data from IBC, PNNL, and SRTC). This data was obtained from traditional batch contact testing for both SuperLig® 644 and SuperLig® 639 resins. In response to this observation, an improved method for determining true equilibrium K_d data (i.e., isotherm data) and particle kinetics data was undertaken. Testing protocols for measuring equilibrium and particle kinetics behavior have differed over time (e.g., contact time, agitation methods, sample sizes, phase ratio, and resin pretreatment) consequently contributing to the observed variability. It is recommended that proposed batch contact testing protocol be verified through limited particle kinetics testing as outlined and demonstrated within this report This verification should be done prior to any batch contact testing.

In developing a particle kinetics apparatus, attention was placed on obtaining a testing method that would provide a platform where reproducible data could be obtained in a cost effective manner. Special attention was also placed on the ability to control the agitation rate where the mass transfer effects of surface film diffusion versus particle pore diffusion could be quantitatively separated. To meet these objectives, a differential column approach was chosen where the differential column housing the small resin bed was placed outside of the vessel containing the liquid of interest. The liquid being tested is forced through the differential column by means of an external pump and recirculates through the column and vessel in a closed loop configuration. During the development of the new kinetics apparatus, several simple kinetics runs were made to address and improve the apparatus' ability to provide reproducible results. The kinetics apparatus discussed within this report can be used to study the behavior of all the resins currently being considered for the removal of cesium and technetium from the low activity waste (LAW) streams, as well as those outside the scope of this work.

Given a kinetics apparatus that can provide meaningful ion-exchange/adsorption behavior for the various resins of interest, the following items can be addressed in a more quantitative way:

- Particle pore diffusion coefficients
- Surface film diffusion coefficients
- "True" equilibrium isotherms
- Potential impact of slower competitors
- Potential impact of chemical degradation

A series of kinetics experiments were performed to demonstrate/confirm the capabilities of the new kinetics apparatus and to create a consistent particles kinetics and equilibrium database for SuperLig® 639 resin in contact with three different simulants. The series of experiments performed (eleven in total) ranged over temperature (i.e., 25, 35, and 45 ºC), simulant composition (i.e., Envelope A (AN-105), Envelope B (AZ-102), and Envelope C (AN-107)), and particle size (i.e., 10-60 mesh, 10-20 mesh, 20-40 mesh, and 40-60 mesh sieve fractions). Experiments in which the flow rate was varied (30 mL/min (12.5 cm/min), 1 mL/min (0.416 cm/min), and 0.5 mL/min (0.208 cm/min)) were performed to provide information about pore and film diffusion characteristics. The resulting database provides key information to be used in the modeling and analyses of technetium removal from LAW feeds from ion-exchange columns packed with SuperLig® 639 resin. The main focus being column performance during the loading phase of the process.

Based on initial scoping tests a maximum 120-hour contact time was chosen and later experimentally verified to be adequate in achieving a "true" equilibrium state on a perrhenate-SuperLig® 639 isotherm. A telescoping sampling time frequency was chosen in such a way as to provide early time data where particle kinetics dominate and late time data to verify equilibrium behavior has been reached. A summary of the perrhenate equilibrium loading levels for SuperLig® 639 is given in Table 1-1.

One set of experiments was performed in which AN-105 simulant at varying temperatures was placed into contact with unsieved SuperLig® 639 resin using the kinetics test apparatus. The results of these experiments are shown in Figure 1-1. The data from the two experiments performed at 25°C (i.e., Exp-1 and Exp-2) illustrates the level of reproducibility achieved when using the kinetics test apparatus and methodology. As expected and shown in Figure 1-1, the adsorption capacity of SuperLig® 639 resin (i.e., the plateau regions at late contact times) drops at higher temperatures. A drop in capacity of approximately 1.5% is observed for every 1ºC increase in contact temperature. Also, the results shown in Figure 1-1 indicate that no appreciable resin degradation or slower competitor effects are occurring over the 120-hour contact period as no decrease in capacity is observed. Thus, a "true" equilibrium point on the appropriate adsorption isotherm has been measured. Results of these experiments also indicate, as expected, that an increase in the rate of pore diffusion is observed with an increase in temperature. This trend is clearly illustrated in the normalized Re concentration curves shown in Figure 4-2 of Section 4.0.

To study the impact of particle diameter on particle kinetics and equilibrium adsorption capacity, kinetics experiments were performed using three sieve fractions of the SuperLig® 639 resin (specifically, 10-20 mesh, 20-40 mesh, and 40-60 mesh). Based on prior information from IBC it was anticipated that the adsorption capacity of SuperLig® 639 particles would not be a function of particle diameter. In addition, it was expected that slower adsorption rates would be observed for particles of larger diameter. These expectations are consistent with the notion that the active adsorption sites are uniformly distributed throughout the pore structure of each particle. As expected and shown in Figure 1-2, the adsorption capacity of SuperLig® 639 is particle size independent (i.e., the plateau regions at late contact times are within the level of

reproducibility achievable), while the rate of perrhenate uptake is slower for the larger sieve fraction samples.

To study the impact of solution composition on particle kinetics and equilibrium adsorption capacity, the results from three simulants (i.e., Envelope A (AN-105), Envelope B (AZ-102), and Envelope C (AN-107)) with varying nitrate-to-perrhenate molar ratios were considered. Based on prior information about the adsorption isotherm (see Hamm et al., 2000b), nitrate is the predominate competitor for perrhenate and the true equilibrium loading levels will depend strongly on the nitrate-to-perrhenate ratio. For the three simulants tested, the approximate nitrate-to-perrhenate ratios varied significantly (i.e., 19,800 for AN-105, 2,700 for AZ-102, and 81,500 for AN-107). Based on this wide range in nitrate-to-perrhenate ratios and the understanding of the perrhenate isotherm, it was expected that loading levels at equilibrium would vary inversely with this ratio. As expected and shown in Figure 1-3, the adsorption capacity of SuperLig® 639 varies inversely with the nitrate-to-perrhenate ratio, and decreases in the order of Envelope B (AZ-102), Envelope A (AN-105), and Envelope C (AN-107). At later contact times the loading levels for Envelopes A and B reach a plateau indicating that a true equilibrium value has been reached where potential degradation or slower competitor effects were not observed. A slight decrease in loading was observed for the Envelope C simulant samples taken at 72 and 120 hours. This is thought to be a sensitivity issue with the ICP-MS analyses (due to organic constituents) rather than degradation or slower competitor effects.

1.4 Quality Requirements

This work was performed in accordance with the RPP-WTP QA requirements specified for work conducted by SRTC as identified in DOE IWO MORSLE60. SRTC has provided matrices to WTP demonstrating compliance of the SRTC QA program with the requirements specified by WTP. Specific information regarding the compliance of the SRTC QA program with RW-0333P, Revision 10, NQA-1 1989, Part 1, Basic and Supplementary Requirements and NQA-2a 1990, Part 2.7 is contained in these matrices.

This work was conducted according to the QA requirements in the following Test Specifications and Task Plans: TSP-W375-01-00023, Rev. 0 (Johnson, 2001a); TSP-W375-01-00021, Rev. 0 (Johnson, 2001b); TSP-W375-01-00022, Rev. 0 (Johnson, 2001c); WSRC-TR-2001-00202, Rev. 0 (McCabe, 2001a); WSRC-TR-2001-00204, Rev. 0 (McCabe, 2001b); and WSRC-TR-2001-00465, Rev. 0 (Saito, 2002). The work requirements described in the Task Plans were subsequently modified in Test Exceptions 24590-WTP-TEF-RT-02-016 and 24590-WTP-TEF-RT-02-010, Revision 1. This work was not required to comply with RW-0333P, Rev. 10. This work does comply with NQA-1 1989, Part 1, Basic and Supplementary Requirements and NQA-2a 1990, part 2.7.

The original Technical Specification QA Requirement drivers were to NQA-1-1994, Basic and Supplementary Requirements, and to RW-0333P Revision 8 (if applicable), which was in effect at the time the specifications were issued (2/01). The tasks, however, were conducted in accordance with the newer RPP-WTP QA requirements as specified in DOE IWO MOSRLE60, dated 6/2001.

SRTC has provided matrices to WTP demonstrating compliance of the SRTC QA program to the newer requirements as specified by WTP. Specific information regarding the compliance of the SRTC QA program with RW-0333P, Revision 10, NQA-1 1989, Part 1, Basic and Supplementary Requirements and NQA-2a 1990, part 2.7 is contained in these matrices. The QA requirements specified in the Task Technical and Quality Assurance Plans were to these newer QA requirements. No additional QA requirements were required nor implemented in this work.

1.5 Issues

No issues of plant significance were identified in this work.

Table 1-1. Perrhenate equilibrium loading levels determined for SuperLig® 639 resin (batch I-R2-03-02-20-45).

Simulant	Temperature (°C)	Particle Sieve Fraction (mesh)	ReO_4^- Loading (mmol/g)
AN-105	25	unsieved	1.11E-02
AN-105	25	unsieved	1.13E-02
AN-105	35	unsieved	9.97E-03
AN-105	45	unsieved	7.95E-03
AN-105	25	40-60	1.06E-02
AN-105	25	20-40	1.03E-02
AN-105	25	10-20	1.07E-02
AN-105 [a]	25	unsieved	1.14E-02
AN-105 [b]	25	unsieved	1.14E-02
AZ-102	25	unsieved	3.59E-02
AN-107	25	unsieved	3.94E-03

[a] Flow rate = 1 mL/min (0.416 cm/min)
[b] Flow rate = 0.5 mL/min (0.208 cm/min)

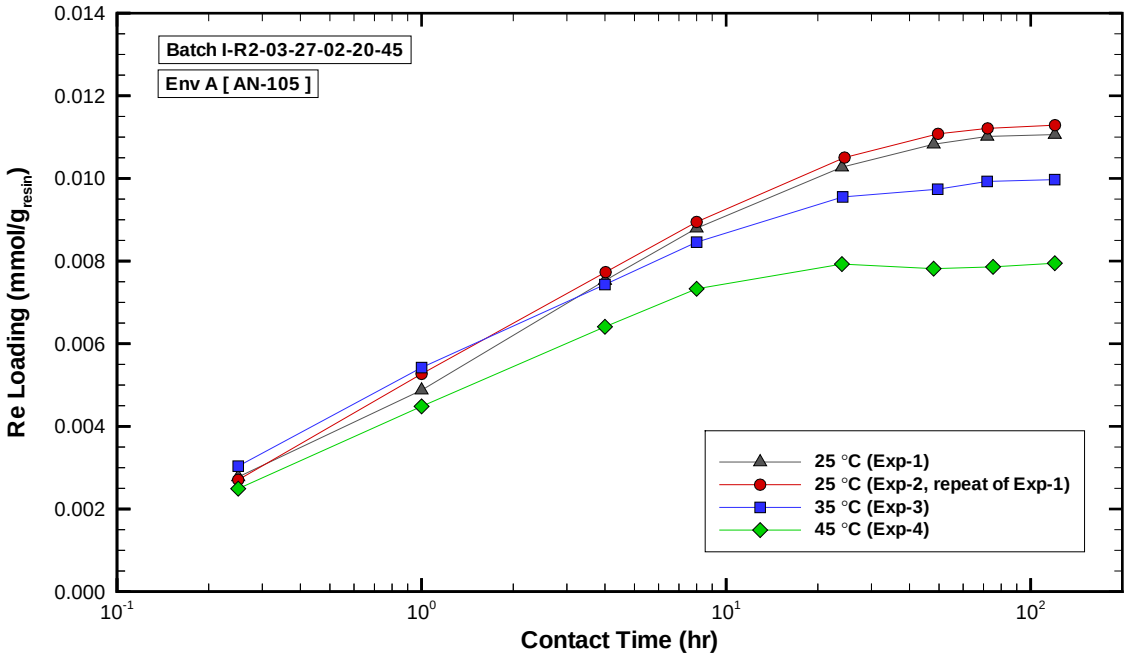

Figure 1-1. Transient rhenium loading levels for the three contact temperatures studied.

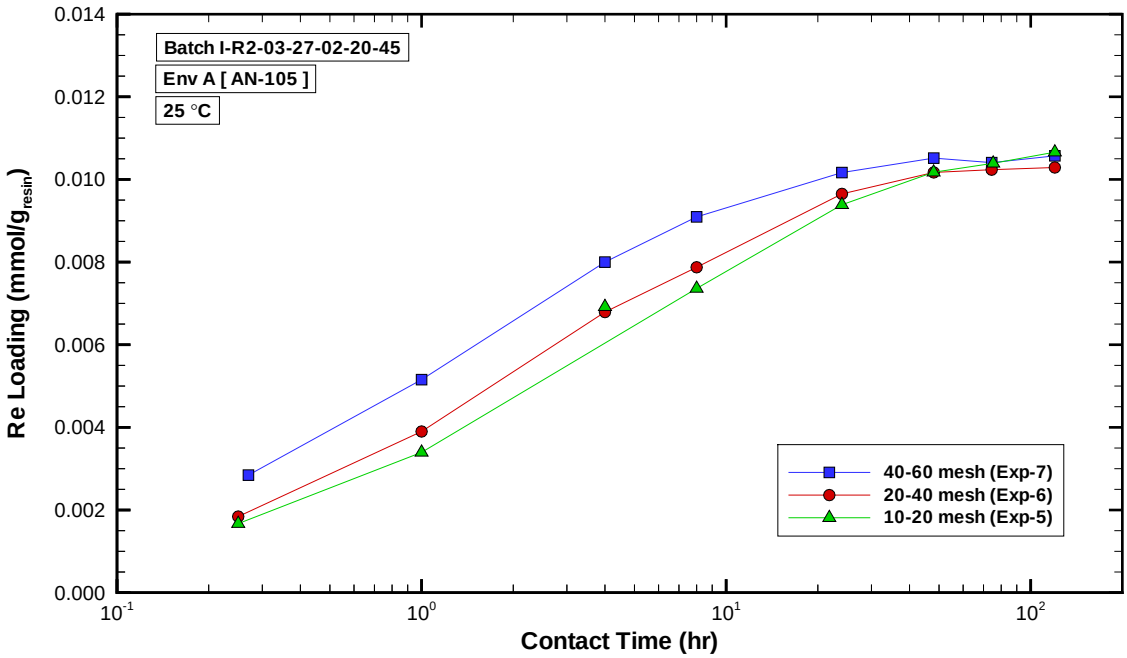

Figure 1-2. Transient rhenium loading levels for the three sieve fractions studied.

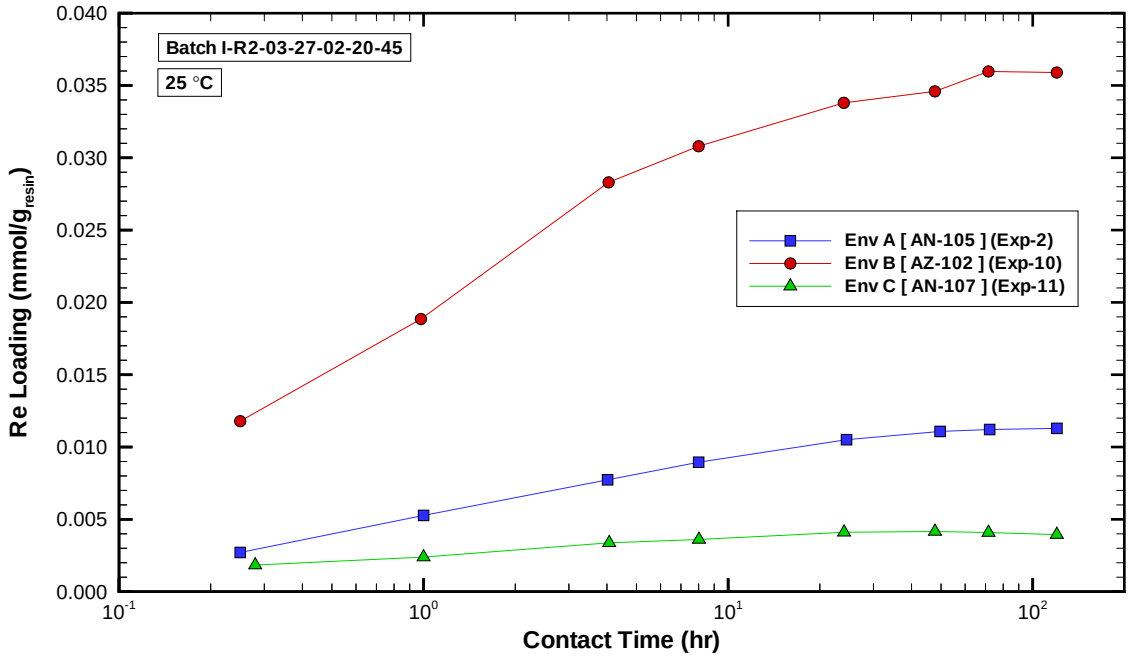

Figure 1-3. Transient rhenium loading levels for Envelope A, B, and C simulants.

(This Page Intentionally Left Blank)

2.0 Background and Introduction

2.1 Overview

Millions of gallons of radioactive waste were produced as a by-product of the production of nuclear weapons at various government sites across the United States. The current legacy waste inventory has essentially been reduced to two main sites (Hanford, WA and Aiken, SC) which are currently managed by the Department of Energy. Separate waste treatment processes have been developed for each site due to differences in waste composition and regulatory requirements for ultimate disposal. Development of the Hanford waste treatment strategy was originally contracted to BNFL, Inc. Based on limited initial testing and extensive nuclear waste processing experience, a treatment process was developed that included the following basic steps: 1) separation of low volume, high activity solids from high volume, lower activity supernate, 2) treatment of the supernate for the removal of specific radionuclides (strontium, transuranics, cesium, and technetium) using precipitation and ion-exchange technologies, 3) evaporation of the bulk decontaminated low activity supernate, 4) vitrification of the decontaminated and concentrated supernate to generate low activity waste glasses, and 5) vitrification of high activity solids and ion-exchange eluate solutions to generate concentrated high activity glasses. This treatment scheme was designed to minimize the volume of high activity waste requiring disposal.

Extensive testing was conducted in support of the original BNFL design for the Hanford waste treatment plant at the Savannah River Technology Center (SRTC) in Aiken, SC and at Pacific Northwest National Laboratory (PNNL) in Hanford, WA, during the period from 1998-2001. The test results indicated that the conceptual design plan was adequate and the Department of Energy subsequently contracted Bechtel to design, build, and perform initial operations of the waste treatment plant at Hanford. The River Protection Project - Waste Treatment Plant (RPP-WTP) for treatment of the Hanford radioactive waste is currently under construction. Final design validation and process optimization tests are continuing at SRTC and at PNNL during the design and construction phase.

The initial plant treatment schedule focuses on 10 waste storage tanks located at Hanford which have been categorized into four general waste types (or Envelopes). Envelopes A-C refer to liquid supernate samples that vary in chemical composition, while Envelope D refers to solids (sludge) primarily isolated from tank heels. Extensive testing has been conducted on actual samples in each waste category that were retrieved from the tanks. In order to minimize costs associated with sample isolation, transfer, and handling, recipes have been developed at SRTC and PNNL to prepare nonradioactive simulants of various tank samples based on analysis data from actual samples. Supernate simulants have been developed for several specific waste tanks and are being used for testing throughout the RPP-WTP test program. All tank supernate compositions are dominated by sodium salts (nitrate, nitrite, hydroxide, and aluminate are the dominant counterions), which are generally present in high concentrations (2-10 M Na^+). All waste samples are highly caustic. Minor waste constituents are extensive in number and type and the targeted radionuclides for removal are present at concentrations that are several orders of

magnitude lower than the concentrations of the primary constituents. These conditions require treatment technologies that are highly selective. The baseline treatment methodology for the supernate involves evaporation or dilution to near 5 M Na^+ followed by precipitation for removal of radioactive strontium and transuranic elements (only needed for Envelope C) and ion-exchange treatment for the removal of cesium and technetium.

This report summarizes the results of recent tests conducted at SRTC with SuperLig® 639 resin in support of the RPP-WTP design. SuperLig® 639 resin is the chosen technology for removal of Tc-99 from the waste samples. Technetium primarily exists in the waste as pertechnetate ion. SuperLig® 639 resin is highly selective for pertechnetate ions and has previously been demonstrated to satisfy design requirements for the removal of technetium from actual Hanford waste samples. Extensive testing has also been conducted with SuperLig® 639 resin using waste simulants containing sodium perrhenate as a chemical surrogate for sodium pertechnetate. Previous testing has shown that pertechnetate ion uptake by SuperLig® 639 resin is higher than perrhenate uptake under identical conditions by approximately 70% (Hamm et al., 2000). However, the diffusional properties of these two species in solution are known to be quite similar (Rard, 1991, Reid et al., 1977, Perry, 1973). Modeling efforts have demonstrated that simulant tests conducted with perrhenate ion can be utilized to predict resin performance with actual samples containing pertechnetate ion (Hamm et al., 2000b) after correction for the differences in loading levels between these two species.

Due to the proprietary nature of SuperLig® 639 resin, only limited information is available with regard to the chemical composition, structure, and function of the material. The current understanding of pertechnetate ion uptake by SuperLig® 639 resin includes the following concepts. The resin is prepared by attachment (presumably covalent molecular attachment) of a proprietary reagent to preformed commercially purchased polystyrene beads. The bound reagent is highly selective for pertechnetate ion in solutions (both caustic and acidic) containing high sodium ion concentrations. The number of ligand sites occupied is believed to be dependent upon the total ionic strength, composition, and concentrations of various ions of interest in the liquid phase. The resin does not behave as a traditional ion-exchange material. Rather, pertechnetate ion uptake occurs by extraction of neutral ion pairs from solution, with sodium pertechnetate presumably being the dominant bound species. The primary competitor for sorption sites on the resin is believed to be sodium nitrate, which is present at concentrations that are orders of magnitude larger than the pertechnetate ion concentration. Bound pertechnetate ion can be eluted from the resin with water. Sorption sites on the resin after elution are considered to be unoccupied by sorbing species. It should be noted that much of the above information was obtained through informal discussions with the resin manufacturer. Knowledge of the molecular structure of the bound reagent would obviously allow for much greater insight with regard to the properties of this material and increase confidence in the above conceptual details of the sorption process.

Perrhenate sorption kinetics tests have been performed using a differential column approach with SuperLig® 639 resin and simulants of Hanford waste tanks 241-AN-105, 241-AZ-102, and 241-AN-107. These waste tanks have been categorized as Envelope A, B, and C waste types, respectively. Column tests (both lab-scale and pilot–scale) have been conducted at SRTC to

evaluate the impacts of solution flow rate, resin bed geometry, temperature, and solution composition upon rhenium breakthrough performance (King et al., 2000, Steimke et al., 2000, King et al., 2003). The collective column test results serve as primary data sources for the model methodology used to predict full-scale column performance. The baseline flow rate of 3 BV/hr for the SuperLig® 639 columns in the plant design is sufficiently fast that sorption kinetics significantly impacts the shapes of the technetium (or rhenium) breakthrough profile during column loading. Experimental determination of the fundamental diffusional parameters (as described by film and pore diffusion coefficients) impacting sorption kinetics with SuperLig® 639 resin is important for accurate, validated column performance modeling.

The rate of uptake of specific ionic species (pertechenate or perrhenate ions) is believed to be primarily determined by liquid phase diffusion processes. Diffusion in a packed bed immersed in a liquid phase can be categorized by three distinct processes: bulk, film, and pore diffusion. Bulk diffusion of a given ionic species in solution is determined from the known free diffusion in water, which is strongly temperature dependent. In solutions containing other dissolved species, corrections to the free diffusion value must be made for changes in solution viscosity and ionic activities. In a constant flow environment, such as an ion-exchange column, the contribution of diffusion within the bulk liquid phase is small. A boundary layer exists within the liquid phase near the resin particle, which separates the bulk liquid phase from the liquid film surrounding the resin particles. Liquid flow characteristics vary dramatically across this boundary. Transport of ionic species across this boundary is directly dependent upon the liquid phase superficial velocity, with higher flow resulting in more rapid transport. Within the film surrounding the resin particles, diffusion of ionic species is assumed to occur under relatively static flow conditions through the pores within the particle to the active sorption sites. For SuperLig® 639 resin, pore diffusion is considered to be quite slow relative to the other mechanistic steps and to primarily determine the rate of uptake of pertechnetate or perrhenate ions from Hanford waste simulants. The actual sorption process across the liquid-solid phase boundary to the active resin sites is believed to occur quite rapidly and to have a negligible contribution to the overall rate of uptake.

We have developed a method using a differential column approach for the measurement of perrhenate sorption kinetics with SuperLig® 639 resin under controlled, dynamic flow conditions. By careful selection of solution flow rates shown to be sufficiently fast to minimize the contributions of film diffusion to perrhenate uptake, sorption kinetics as primarily determined by the particle pore diffusion could be directly measured. Separate experiments were also conducted at slower flow rates to quantify the film diffusion characteristics of this system. Tests were conducted with AN-105 simulant containing perrhenate ion varying the resin particle size, solution temperature, and flow rate. Additional tests were conducted with AZ-102 and AN-107 simulants to evaluate the impacts of solution composition. The data will be utilized to evaluate model predictions of SuperLig® 639 column performance under a variety of operating conditions.

2.2 Motivation Behind Kinetics Testing using a Differential Column Approach

Based on inconsistencies and the lack of obtaining reproducible data (typically represented by distribution coefficients, K_d) during batch contact testing of ion-exchange materials with Hanford waste simulants, a study was undertaken at SRTC to develop a different test method for these determinations. The outcome of that study was the creation of a differential column approach where both key kinetics information and true equilibrium data can be obtained during a single experimental run. In this chapter, a discussion is provided about various motivational factors that played a role in determining the specific apparatus chosen (referred to as a differential column approach). In later chapters, the application of this new testing method is presented for the sorption behavior of rhenium (in its perrhenate form) onto SuperLig® 639 resin.

2.2.1 Particle Kinetics versus Multiple Batch Contact Testing

The current approach to modeling of ion-exchange columns for the RPP-WTP is discussed in detail by Hamm et al. (2000a, 2000b). To take into account the various mechanisms for transport and sorption of an ionic species as it travels down an ion-exchange column, a porous particle solute transport formulation is being used (i.e., the VERSE-LC liquid chromatography algorithm by Whitley and Wang, 1996). For this class of column models, five basic aspects of the ion-exchange column are addressed. In order of their importance with respect to predicting exit breakthrough curves for the systems of interest, they are:

- **Bed Definition** (high impact) – column size, geometry, and resin mass;
- **Adsorption Isotherms** (high impact) – resin affinities for the various competing ions of interest;
- **Pore Diffusion** (moderate impact) – intra-particle mass transport by pore diffusion to available surface sites (includes particle shape impacts);
- **Film Diffusion** (low impact) – liquid mass transport by film diffusion across the particle-to-bed boundary; and
- **Axial Dispersion** (low impact) – mass transport along the column by axial dispersion.

The above stated levels of impact are based on sensitivity studies and are relative values. Mechanisms such as surface migration or sorption rates across the liquid-solid phase boundary are not included in the column models since their impacts are considered to be negligible or already indirectly incorporated into the other features during the parameter estimation process. A simple graphical representation of the various transport mechanisms listed above and considered to be important for the resin of interest is shown in Figure 2-1.

Focusing on the particle kinetics (i.e., the rates associated with film diffusion, pore migration, and surface reactions), analyses presented by Hamm et al. (2000a, 2000b) have demonstrated that for SuperLig® 639 and SuperLig® 644 resins the overall mass transfer rates are primarily pore diffusion limited. To experimentally determine the "effective" pore diffusion coefficients

for the species of interest, either multiple batch contact tests or a kinetics type of test must be performed.

When performing a traditional batch contact test, a fixed amount of "fresh" dry resin is placed into direct contact with a fixed amount of liquid solution (i.e., phase ratio of the test being defined as the liquid solution volume to dry resin mass, ml/g). The mixture is agitated for a specified amount of time maintaining the mixture at a constant temperature. The amount of dry mass of resin, liquid-phase composition, and agitation rate are held constant. At some selected point in time, the batch contact vial is removed from agitation and the liquid-phase concentrations of the various species of interest are measured. Agitation of the mixture is generally performed by some sort of shaking mechanism (e.g., orbital shakers).

The mass transfer process occurring during the batch contact period is graphically represented in Figure 2-2. The isotherm curve (shown in red) represents the equilibrium surface concentration (Q_i) of a given species, i, versus its liquid-phase concentration (c_i). The straight line (shown in blue) represents the actual surface versus liquid-phase concentrations as a function of time (i.e., typically referred to as the operating line whose slope is the negative of the phase ratio). For a constant phase ratio this line remains linear throughout the contact period. The case illustrated in Figure 2-2 assumes the resin material to be initially void of the species of interest and that equilibrium conditions are reached by ~120 hrs of contact. The point of intersection between the isotherm and the operating line represents the ultimate end (equilibrium) loading state for the resin under the test conditions measured. A K_d value can also be estimated as shown in Figure 2-2 at any point along the operating line (i.e., transient to equilibrium value). The maximum achievable loading on the resin for the particular liquid solution is shown and is referred to as the "apparent ionic capacity".

In Figure 2-2 the isotherm shown represents an isotherm for a resin material which does not chemically degrade while in contact with the selected testing solution. For some resin materials the resin's loading capability degrades after sustained exposure to the testing solution. Chemical degradation can significantly complicate the kinetics data if the degradation rates are large enough to have appreciable impacts on capacity at exposure times where particle kinetics is important. This is illustrated in Figure 2-3 showing the periods where particle kinetics, apparent equilibrium, and chemical degradation (or slower competitors) each dominate. To have a successful understanding of particle kinetics, a region where an apparent equilibrium is established should separate particle kinetics from chemical degradation or slower competitor effects. The isotherm shown in Figure 2-2 corresponds to the isotherm generated during the region of apparent equilibrium shown in Figure 2-3.

When performing multiple batch contact testing, a series of resin samples (generally of fixed amount) are placed into direct contact with the liquid solution of interest and are agitated for a specified amount of time at the same temperature. At selected points in time, each individual batch contact vial is removed from agitation and the liquid-phase concentrations of the various species of interest are measured. Variations in the chemical performance of a resin may exist due to the manufacturing process and/or manner of storage employed (e.g., for SuperLig® 644 particles, prior testing has indicated that the apparent capacity of the resin is strongly particle size dependent). When using the multiple batch contact approach to obtaining a set of kinetics

data, a risk associated with resin sampling variance can exist. Such sampling differences can result in inconsistent kinetics data sets. To eliminate this potential source of error, the kinetics testing of a single batch of resin is preferred. Here, sample draws from the liquid solution are taken at selected time intervals where the amount of liquid withdrawn should be kept as small as possible such that the phase ratio is not significantly altered (e.g., 1% or less per draw).

One other source of error can occur due to uncertainties associated with the degree of agitation each batch contact vial is experiencing. The typical methods for agitation focus on some sort of mechanical shaking. The degree of agitation can vary depending upon the density difference between the liquid and resin phases, as well as resin particle sizes. Mechanical shaking results in complex time varying flow patterns where estimates of the average agitation rates can vary. To minimize this particular source of error, a method of controlling a known flow rate passing over the resin sample is preferred.

2.2.2 The Differential Column Approach

As indicated above, to minimize/eliminate sources of potential errors, a kinetics experimental design that used the same resin sample being exposed to solution under a controlled flow rate was desired. To accomplish these two objectives, a differential column approach was chosen. A simple schematic of the approach chosen is illustrated in Figure 2-4. Here a large phase ratio is used where several small liquid samples can be withdrawn for analysis without resulting in significant changes in the phase ratio. The resin is maintained in a fixed resin bed geometry of low L/D (i.e., a differential column) where the solid surface and liquid phase concentrations are relatively uniform for every particle comprising the bed. To provide a known, fixed, and controllable flow rate over the differential column, the bed is placed outside of the solution vessel where a pump providing pulseless flow is used. To minimize transport lag-times to and from the solution vessel and the differential column, small transport lines of limited length are used. The contents of the solution vessel (i.e., simulant bottle) are maintained well-mixed through mechanical stirring action and behaves similar to a continuous stirred tank reactor (CSTR). The temperature of the entire experimental setup is maintained at some specified value throughout a particular test run.

2.2.3 SuperLig® 639 Absorption Behavior

The differential column contained within the kinetics experimental setup is designed to handle resin material whose particle diameters range from approximately 210 to 2000 mm (i.e., 70-10 mesh). Both SuperLig® 639 and SuperLig® 644 resin particle size distributions (PSD) are within this design range. Within this report, kinetics results for a specific batch of SuperLig® 639 are presented where the capabilities of the experimental setup are demonstrated. SuperLig® 639 is a specifically designed resin for the removal of trace amounts of pertechnetate from high alkaline waste streams. The active SuperLig® 639 ligands are placed on the surfaces of a near spherical polystyrene bead (i.e., distributed over the outer surface of a bead and on the inter-surfaces of the bead's internal pore structure). These beads exhibit only limited swelling and shrinking characteristics (i.e., observed 1-2% over the entire pH and ionic strength range of interest).

The SuperLig® 639 resin selectively adsorbs technetium (and the chemical surrogate rhenium) only in its oxide form of pertechnetate (or perrhenate). The major anion competitor is nitrate. The adsorption process is believed to be based on a neutral ligand site where the sodium and potassium compounds formed with these various anions are involved. For example, for a rhenium based waste solution in contact with the SuperLig® 639 resin the following four mass-action processes would apply:

$$[\overline{L}] + [Na^+] + [ReO_4^-] \xleftrightarrow{K_{eq,1}} \left[\overline{L - NaReO_4}\right], \quad (2\text{-}1)$$

$$[\overline{L}] + [K^+] + [ReO_4^-] \xleftrightarrow{K_{eq,2}} \left[\overline{L - KReO_4}\right], \quad (2\text{-}2)$$

$$[\overline{L}] + [Na^+] + [NO_3^-] \xleftrightarrow{K_{eq,3}} \left[\overline{L - NaNO_3}\right], \quad (2\text{-}3)$$

$$[\overline{L}] + [K^+] + [NO_3^-] \xleftrightarrow{K_{eq,4}} \left[\overline{L - KNO_3}\right], \quad (2\text{-}4)$$

where the bars imply the solid surface phase. Four similar mass-action processes apply for technetium based waste solutions. The thermodynamic equilibrium constants are reasonably temperature dependent, as can be seen in the kinetics results to follow and from column elution studies at varying temperatures. The thermodynamic equilibrium constant for the first mass-action equation shown above, Eq. (2-1), can be expressed as (assuming the surface adsorption sites behave ideally):

$$K_{eq,1}(T) = \left[\frac{\left[\overline{L - NaReO_4}\right]}{[\overline{L}][Na^+][ReO_4^-]}\right]\left[\frac{1}{\gamma_{Na^+}\gamma_{ReO_4^-}}\right]. \quad (2\text{-}5)$$

In Eq. (2-5) the terms contained within the first bracket represent the equilibrium concentrations of pertinent species in solution and on the resin surface, while the terms within the second bracket represent the activity coefficients for the liquid-phase species.

As indicated by the equilibrium constant and the various mass-action equations shown above, elution of the SuperLig® 639 resin will be predominately controlled by the eluate's temperature and concentration level present for sodium, potassium, nitrate, and perrhenate. A total ionic strength effect can be seen since, ionic strength is impacted primarily by concentration levels of these species and the compositional effect associated with solution phase nonidealities (i.e., plays a part to a lesser extent). The impact of varying pH does not have a direct impact, but can have an indirect impact by altering the total ionic strength of the solution.

2.2.4 Perrhenate Loading on SuperLig® 639

An isotherm for the adsorption of total perrhenate onto SuperLig® 639 resin represents the equilibrium solid-phase concentration of perrhenate as a function of its liquid-phase concentration for a specified temperature. A simple algebraic form of the perrhenate adsorption isotherm for SuperLig® 639 resin has been developed by Hamm et al. (2000b). Based on this simplified form, for perrhenate on the SuperLig® 639 resin the isotherm can be expressed as:

$$Q = \frac{\overline{C}_T c_f}{c_f + \beta} \tag{2-6}$$

where

- Q - perrhenate loading on resin (mmol of Re/gram of dry resin)
- $\overline{C}_T$ - total perrhenate adsorption capacity (mmol of Re/gram of dry resin)
- c_f - liquid-phase rhenium concentration at equilibrium (final conc.) [M]
- β - beta parameter reflecting competitor nitrate, impact [M]

and the beta parameter for perrhenate becomes dependent upon the nitrate feed concentration expressed as:

$$\beta = \widetilde{K}_{21} c_{NO_3^-} \tag{2-7}$$

where

- $\widetilde{K}_{21}$ - selectivity coefficient for perrhenate versus nitrate competition (-)

The beta parameter for our purposes will be approximately constant, since the nitrate concentration remains fairly constant over the entire testing cycle (i.e., initially high abundance of nitrate present compared to the total number of active ligands within the differential bed).

The total perrhenate adsorption capacity, $\overline{C}_T$, represents the total number of sites that can be occupied at a specified set of conditions (i.e., generally less than the total number of assessable ligands). As Eqs. (2-1) through (2-4) indicate, this value is strongly dependent upon the composition of the solution respect to Na^+ and K^+ levels. Basically, at practical Na^+ and K^+ concentration levels, a modest fraction of the available ligands will remain bare (i.e., have unoccupied sites).

The typically referred to equilibrium "K_d" value is related to the isotherm given by Eq. (2-6) as:

$$K_d \equiv \frac{Q}{c_f} = \frac{\overline{C}_T}{c_f + \beta} \tag{2-8}$$

where the K_d value represents the chord of the isotherm at a specified equilibrium liquid-phase perrhenate concentration level.

2.2.5 Kinetics Data Reduction and Interpretation

Traditionally, a solid-phase loading (i.e., either a transient or equilibrium value), as represented by either a Q or K_d value, is computed using a mass balance for the species of interest (i.e., here perrhenate). For example, K_d and Q values can be computed using the relationships:

$$K_d(t) = \frac{\Delta c(t)}{c_f(t)}\phi \tag{2-9}$$

$$Q(t) = K_d(t)c_f(t) \tag{2-10}$$

where

$$\Delta c(t) = c_i - c_f(t) \quad ; \quad \phi = \frac{V_{soln}}{m_d}; \quad m_d = Fm_i$$

and
- $K_d(t)$ - distribution coefficient at time t (ml/g)
- c_i - initial ReO_4 liquid-phase concentration (M)
- $c_f(t)$ - ReO_4 liquid-phase concentration at time t (M)
- m_d - mass of oven-dried resin (g)
- m_i - mass of filter-dried resin (g)
- F - F-factor for conversion from filter-dried to oven-dried resin mass (-)
- V_{soln} - volume of liquid-phase sample (ml)
- ϕ - phase ratio (liquid-to-resin) (ml/g)
- $\Delta c(t)$ - reduction in liquid-phase ReO_4 concentration at time t (M)

Equations (2-9) and (2-10) above assume that the phase ratio remains essentially constant over the time period of interest.

During a single kinetics run, the liquid-phase concentration of Re (assumed to be present only in its ReO_4 form) is measured at several points in time. At each measurement point in time, a transient Re K_d value and a Re Q value can be computed using Eqs. (2-9) and (2-10), respectively.

When comparing kinetics results from one test setup to another, sometimes it is useful to compare normalized concentrations versus the actual measurement concentration values. For example, when comparing a repeat test where the initial solution concentration has a slight difference or a slight difference in phase ratio exists, a normalized concentration profile tends to minimize such differences. Also, to highlight the unique kinetic differences between tests (e.g., when looking at the impact of particle size), focus should be made on the early contact times. Since the pore diffusional process is somewhat exponential in nature, a semi-log plot of normalized concentration versus contact time is recommended. In the results to be discussed in a later chapter, the following definition of normalized solution concentration is used:

$$\eta(t) = \frac{c_i - c_f(t)}{c_i - c_f^{min}} \tag{2-11}$$

Here, typically the minimum measured solution concentration corresponds to the last measurement point in time. Under these conditions, the normalization represents the approach to

equilibrium where at equilibrium a value of unity is achieved. If degradation or slower competitors exists, the minimum occurs at some intermediate point in time.

Within the complicated pore structure of the resin particles we assume that net fluid motion is approximately zero resulting in equal-molar counter-diffusion. "Effective" binary diffusion coefficients based on Fick's law are assumed where surface migration is considered negligible. Due to the confining nature of molecular diffusion through a pore structure versus open "free-stream" diffusion, some level of reduction is expected resulting from bends along the pore paths that are generally accounted for by a particle tortuosity factor (Smith, 1981; Froment and Bishoff, 1979) defined as:

$$D_{pi} = \frac{1}{\tau} D_{\infty i} \tag{2-12}$$

where

D_{pi} - species pore diffusion coefficient (cm^2/min)
$D_{\infty i}$ - species free-stream diffusion coefficient (cm^2/min)
τ - tortuosity factor for pores within specific particles (-)

Typical values for catalyst particle tortuosity are between 1 and 10. Generally, this tortuosity factor is a unique geometrical property of the resin particles and should be determined empirically based on an appropriate type of kinetics testing. Under high flow rate conditions the particle kinetics is dominated by pore diffusion (i.e., negligible film resistance to mass transfer at the outer particle surface) and the time varying measured solution concentrations provide an indirect measurement of a species pore diffusion coefficient. As discussed by Hamm et al. (2000a, 2000b, and 2002), the tortuosity factor can be approximated using the transient concentration data and the VERSE-LC code.

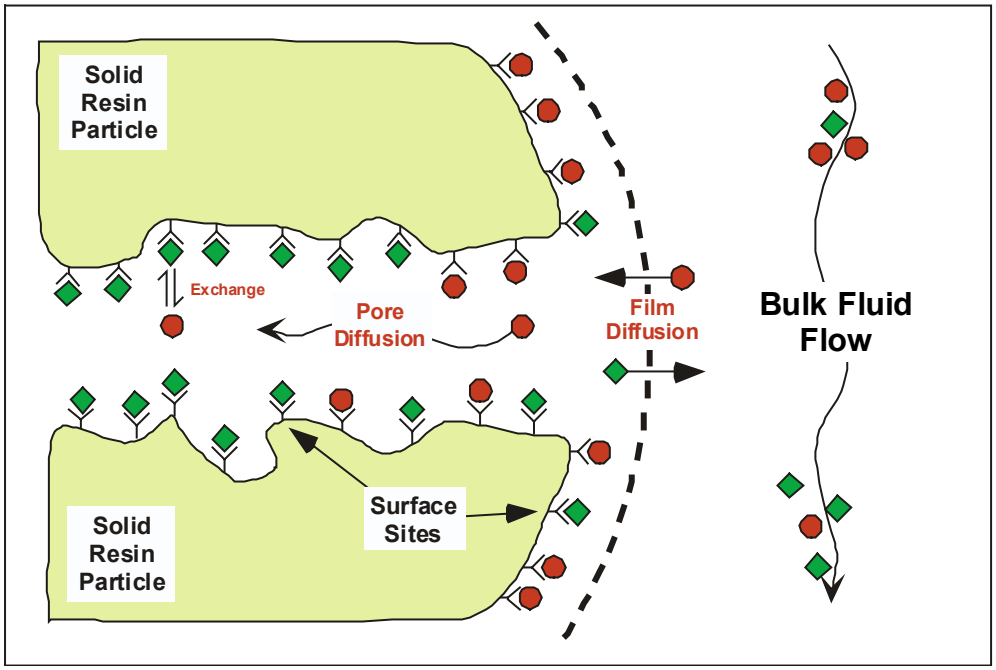

Figure 2-1. Graphical representation of the various mass transport mechanisms considered important for the ion-exchange/adsorption resin of interest.

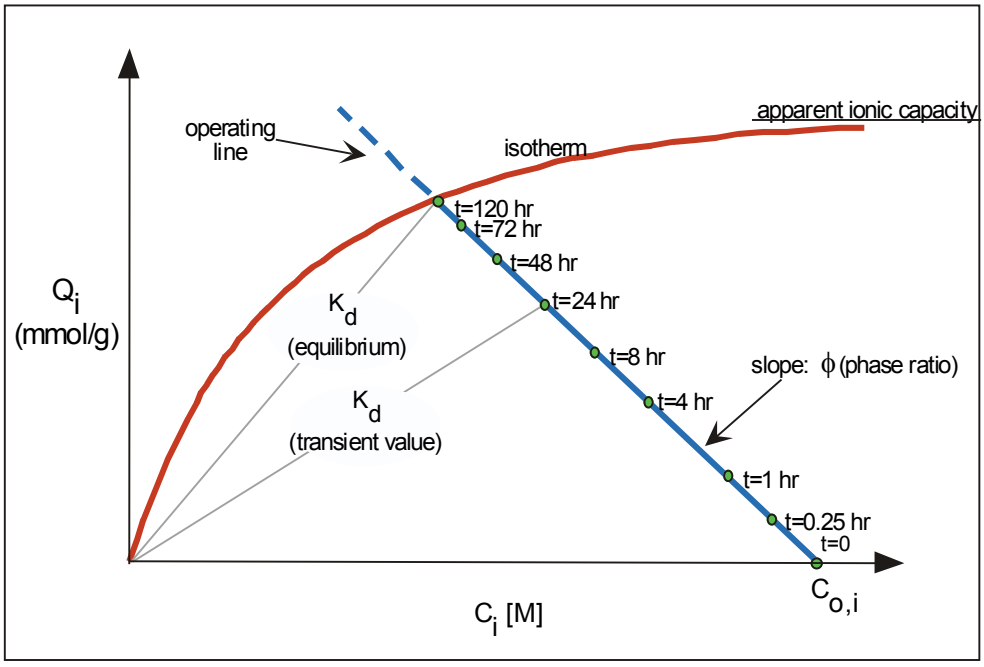

Figure 2-2. Graphical representation of the differential column behavior during a loading test. Liquid-phase species concentration is measured at selected points in time, while the solid-phase species loading levels are computed based on a mass balance equation.

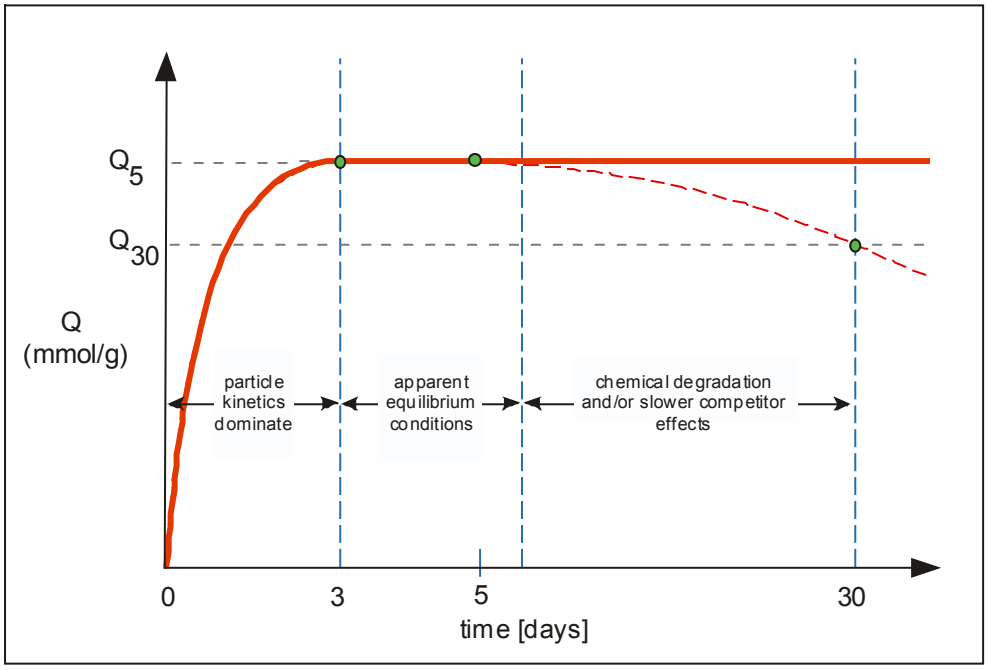

Figure 2-3. Typical resin loading characteristics illustrating the regions where particle kinetics, apparent equilibrium, slower competitors, and chemical degradation tend to dominate. (Dashed red line represents degradation and/or slower competitor effects.)

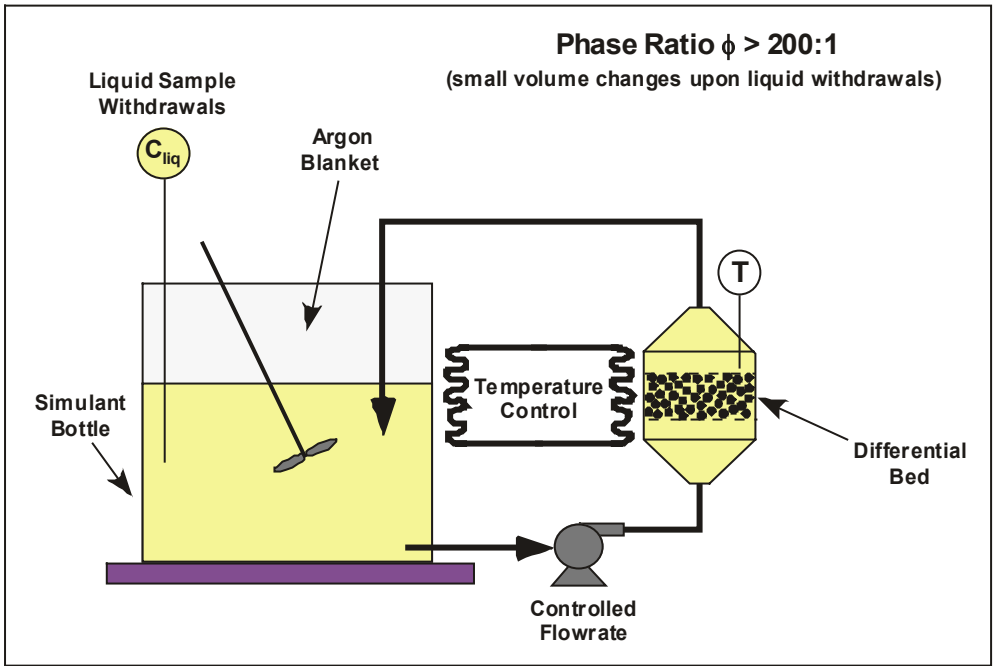

Figure 2-4. A simple schematic representation of the differential column and peripherals. Typically, the phase ratio is high and the volume reductions associated with liquid sample withdrawals are small.

3.0 Experimental

3.1 Resin Handling, Properties, and History

The SuperLig® 639 resin used in all experiments was isolated from the as-received one-gallon bottle containing resin from IBC batch I-R2-03-27-02-20-45 received April 2002. The bottle was approximately 75% full with very little water above the resin. In an effort to minimize oxidation and/or degradation, the resin remained wet or damp (filter-dried) throughout experimentation.

3.1.1 Resin Isolation and Conditioning

To insure homogeneity within the resin sample, the as-received one-gallon plastic bottle was gently tumbled immediately prior to the sample isolation. The sample was removed using a ladle, transferred to a separate plastic bottle and covered with deionized (Millipore®) water. Deionized water was also added back to the one-gallon bottle.

Conditioning of the resin was performed by carefully decanting the water above the resin and replacing it with a volume of deionized water that was 10 times the volume of the resin. The bottle was loosely capped and placed in a 65°C water bath for 24 hours. The water was then decanted from the resin and the resin was washed with three aliquots of deionized water, each of which were two times the volume of resin. The conditioned resin was stored in a plastic bottle with a volume of deionized water equal to approximately two times the resin volume.

3.1.2 F-factor Determination

All kinetics experimentation was carried out using damp (filter-dried) resin, and an F-factor determination was performed immediately prior to the packing of each differential column. The F-factor, in this case, is a measure of the water content of the damp (filter-dried) resin, and is used to calculate the dry mass of resin in the column.

For each differential column experiment, the bottle containing the indicated conditioned resin under water was gently tumbled and swirled to suspend and homogenize the resin. Approximately 10 mL of resin was quickly transferred to a 150-mL Nalgene® 0.45-micron nylon filter cup. To minimize the amount of air pulled through the resin, the filter cup was covered with a piece of latex secured by a rubber band. The excess water was removed using vacuum at 600 mm Hg for 10 minutes. Timing was initiated when all visible water was removed from the resin. Duplicate 0.1 g samples were weighed into separate oven-dried 100-mL beakers. Each beaker was covered with an oven-dried watch glass and placed in a vacuum oven at 600 mm Hg and 50°C for 24 ± 0.5 hours. The samples were cooled in a desiccator then weighed. The samples were returned to the oven for at least one hour, cooled, then weighed again. This procedure was repeated until three masses were obtained which varied no more than 0.01 grams.

The F-factor (F) is defined by the equation

$$F = \frac{m_d}{m_i} \quad (3\text{-}1)$$

where

m_d - oven-dried resin mass

m_i - filter-dried resin mass

The F-factors obtained using this method were very consistent. Table 3-1 shows that changes in the isolation date (isolation from the as-received one-gallon bottle), conditioning date, and particle size (unsieved versus wet-sieved) had little or no impact on the F-factors. The consistency in F-factor values also supports the idea that sampling errors within the same resin batch are not an issue.

3.1.3 Particle Size Distribution

In an effort to correlate results from kinetics experiments using unsieved resin with those investigating particle size dependency, the sample of resin isolated and conditioned 08/23/02 was used in all kinetics experimentation with the exception of Experiment 1. As per Task Plan WSRC-TR-2001-00202 (McCabe, 2001), kinetics experiments investigating particle size dependency were to be performed using three resin sieve fractions. To avoid ambiguity, the three sieve fractions included all particle sizes contained within the unsieved portion of the resin. The conditioned resin was wet-sieved into fractions using ASTM standard sieves as described below. To confirm particle size distribution, Lasentec® and Mictrac® analyses were employed.

- **Wet Sieve Analyses** - The bottle containing the indicated conditioned resin under water was gently tumbled and swirled to suspend and homogenize the resin. Approximately one eighth of the resin was poured into the sieve stack and sprayed with deionized water to fractionate the resin. This procedure was repeated three additional times, yielding approximately 75 mL each of sieved and unsieved resin. The sieve fractions were washed into plastic bottles and stored under deionized water. To minimize loss of resin, the percentage of each resin fraction was visually approximated. Results of the wet-sieve analysis are given in Table 3-2.

After wet-sieving, all three sieve fractions exhibited dynamic floating in water which was not observed in the unsieved portion of the resin. This phenomenon persisted for several weeks and is thought to have had some impact on the perrhenate loading capacity. See Section 4.2 for further discussion.

Sieve sizes were chosen based upon a scoping wet-sieve analysis using approximately 30 mL of the resin sample isolated 04/23/02 and conditioned 05/24/02. Since this resin was not to be used in further experimentation, the sieve fractions were dried to a constant weight and mass fractions were obtained. Results of the scoping wet-sieve analysis are given in Table 3-3.

- **Lasentec® Analyses** – Chord length analyses were conducted on the three sieve fractions as well as the unsieved portion of the resin. See Section 3.3.2. Complete analyses of the 10-20 mesh fraction and the unsieved portion were unattainable due to a portion of this fractions exceeding the 1000 μm detection limit. Results are given in Figure 3-1 and Table 3-4.

- **Microtrac® Analyses** – Microtrac® particle size analyses were conducted on the two smallest sieve fractions. See Section 3.3.2. The maximum diameter detected for this method is 704 μm, which the 10-20 mesh fraction exceeds. In addition, complete analysis of the 20-40 mesh fraction was unattainable due to a portion of this fraction exceeding the 704 μm limit. Results are given in Table 3-4.

3.2 Simulant Preparation and History

Sodium hydroxide solutions utilized for testing were prepared from NaOH pellets and filtered prior to use. Deionized (Millipore®) water was used for all reagent preparations. All simulant solutions were prepared according to procedures published by Eibling and Nash, (2001). The simulant recipes were based on analysis data for Hanford waste tanks 241-AN-105, 241-AZ-102, and 241-AN-107. Reagent grade chemicals were utilized for all preparations.

The AN-105 and AZ-102 simulants were prepared in 2002 specifically for the RPP ion-exchange test program and the simulant compositions included all RCRA hazardous recipe components. The AZ-102 simulant was processed through SuperLig® 644 ion-exchange columns for cesium removal (Hassan et al., 2000). The effluents were composited and then spiked with sodium perrhenate. Immediately prior to use in each kinetics experiment, the simulant solutions were filtered through 0.45 μm Nalgene® Nylon filter units to remove fine particulates that might lead to column fouling. Few solids were visually observed in the solutions prior to filtration or in the filter cups after filtration. The densities and viscosities of the filtered AN-105 and AZ-102 simulants at ambient temperature (20 ± 2 °C) are provided in Table 3-5.

The AN-107 simulant was an archive sample generated in 1999 at the Thermal Fluids Laboratory at SRTC during testing conducted for the previous WTP contractor as part of the strontium/transuranics removal program. The AN-107 sample was originally prepared at 5 M Na^+, but was subjected to caustic adjustment and strontium nitrate and sodium permanganate addition, followed by cross-flow filtration as part of the 1999 test program. The sample was subsequently stored in a 55 gallon drum and then retrieved for ion-exchange testing. The sample did not contain RCRA hazardous components. Based on scoping tests conducted on a portion of the sample that had been spiked with RCRA metals, it was decided that inclusion of these species did not significantly impact ion-exchange testing. Therefore, the archived sample was utilized for subsequent testing without the addition of RCRA hazardous components. The AN-107 sample was green in color (as opposed to the brown color typically observed prior to precipitation) and contained considerable amounts of white solids, which were removed by filtration through 0.45 μm Nalgene® Nylon filter units. The sample was processed through SuperLig® 644 ion-exchange columns for cesium removal (Hassan et al., 2000). The composited effluent was then spiked with sodium perrhenate and filtered again prior to SuperLig® 639

column testing. The density and viscosity of the filtered AN-107 simulant at ambient temperature (20 ± 2 °C) are provided in Table 3-5.

The concentrations of selected species added during initial simulant preparation based on the recipes reported by Eibling and Nash (2001) are provided in Table 3-6. Table 3-7 provides the average measured concentrations of selected species obtained by ICP-ES analyses for each simulant sample prior to SuperLig® 639 kinetics testing, but after the completion of other testing (cesium column and precipitation tests). Note that differences in the data in Tables 3-6 and 3-7 may be due to compositional changes resulting from the cesium and or precipitation testing. A total of eleven kinetics tests were conducted using the simulants indicated in Table 3-7. Individual sample analysis data for the feed solutions is provided in Appendices A-K.

3.3 Equipment

3.3.1 Kinetics Experimental Setup

The entire kinetics experimental setup was based upon a differential column concept as described in Section 2.2. This concept dictates utilization of a thin resin bed exposed to a feed solution with uniform uptake being observed throughout the bed. In essence, this setup was designed to determine resin adsorption properties of a differential cross-sectional area of a typical column during operation. Implementation of this concept required a controlled flow of liquid through the resin bed as well as a controlled temperature throughout the system. Due to the duration of the experiments (120 hours), precautions were taken to minimize resin and/or simulant degradation. The simulant was fed through the column in up flow to minimize the amount of air initially in the system. An argon sparge was continually supplied to the feed. The system remained closed with the exception of a small vent/sampling port as described below. In addition, steps were taken to minimize the volume of simulant held within the transfer lines of the system. A photograph of the complete kinetics experimental setup during operation is shown in Figure 3-2. Descriptions of the individual components are given below.

Differential Column

The jacketed differential column was constructed by the SRTC glass blowers specifically for this task. A close-up photograph of the differential column during operation is shown in Figure 3-3 and Figure 3-4 provides a photograph of an exploded view of the same column. The column and jacket were blown from borosilicate glass, with the main body of the column being ~20 mm in height with a 25 mm ID. Just below the main body, the column flared slightly to an internal thread that supported a recessed PTFE bushing containing a “quick-connect” type fitting. This fitting connected a 1/8” OD and 5/64” ID polyethylene inlet line from the pump. The recession in the bushing held a 40-mesh stainless steel Chromatographic Resin Support® (Dobos, 2002). This screen supported 1-mm borosilicate glass beads which served as flow distributors within the main body of the column. A 5.40 mm glass spacer with a 17.5 mm ID, 25 mm OD was held in the main body of the column between two 100-mesh Chromatographic Resin Supports®. The SuperLig® 639 was weighed into the glass spacer and the resin essentially filled the reservoir. Thus, the bed height was assumed to be 5.40 mm. Assuming complete packing of the spacer yielded a resin bed volume (BV) of 1.3 mL. The column tapered just above the main body to an

internal thread that supported a PTFE connector containing a stainless steel thermometer fitting. A 90° narrow side-arm extended from the taper to an internal thread that supported a PTFE tubing connector. The connected outlet line was 1/8" OD and 5/64" ID polyethylene tubing which returned to the simulant feed bottle as described below. The column jacket had two internal threads, each supporting a polyethylene connector containing a "quick-connect" type fitting. The top and bottom fittings connected 1/4" OD and 7/16" ID Tygon® tubing to the recirculator and jacketed beaker, respectively. All connectors and bushings utilized Viton® or FETFE O-rings to insure a complete seal.

Feed Containment and Sampling

The simulant feed was held within a capped 125-mL polyethylene bottle also containing a 1-inch PTFE stir bar. The cap was drilled with three 1/8" holes equally spaced around the top of the cap for insertion of the argon line, feed line, and return line into the simulant. Each line consisted of 1/8" OD and 5/64" ID polyethylene tubing. In addition, the cap was drilled with a very small hole in the center which served as a vent and sampling port. Samples were withdrawn using a 5-mL plastic syringe fitted with a 4-inch #18 stainless steel needle.

The feed bottle was inserted into a borosilicate glass jacketed beaker containing enough water to equal the level of the simulant. The beaker was fitted with a mushroom-shaped lid to prevent the evaporation of water from the beaker during experimentation. An opening in the center of the lid allowed for a slight protrusion of the feed bottle cap through the lid. The jacketed beaker was placed on a stir plate and held in position with a chain clamp.

Pumps

Experiments 1-7, 10, and 11 were run using Cole-Parmer gear pumps with either PPS or PEEK gears, stainless steel head and PTFE seals. Gear pumps were chosen for use in the kinetics experimentation due to delivery of a smooth, pulseless flow. Scoping studies had been previously performed using a piston type pump where pulsating was observed within the resin bed. This was deemed unacceptable.

Experiments 8 and 9 were run using a Stepdos reduced pulsation diaphragm metering pump with a PVDF head, FFPM valves and gaskets, and PTFE-coated diaphragm. This pump was used to achieve low flow rates for these experiments without observable pulsation.

Inlet and outlet lines for all pumps consisted of 1/8" OD and 5/64" ID polyethylene tubing. Calibration curves depicting the flow rate of water (mL/min) versus pump setting were generated for all pumps prior to kinetics experimentation.

Temperature Control and Monitoring

The differential column and jacketed beaker temperatures were controlled using a Haake DC-5 recirculating unit. The column and beaker were attached in series with the inlet from the recirculator into the bottom of the beaker and the outlet returning to the recirculator from the top of the column. See Figure 3-2. A Neslab Cool Flow CFT-33 chiller was attached to the recirculating unit to help maintain the recirculator temperature in the 25°C experiments. Tubing connecting the column, jacket, and temperature control units was 1/4" OD and 7/16" ID Tygon® tubing.

Scoping experiments indicated there was significant heat loss from the simulant through the stainless steel pump heads at 35°C and 45°C. To eliminate this problem the pump heads were wrapped with a 4'x 1/4" heat tape controlled by an attached mini-controller. The heat tape was wrapped with insulating web and held in place with heat resistant tape. Heat loss was minimized in the 25°C experiments by wrapping the stainless steel pump heads with insulating web held in place by heat resistant tape.

The simulant temperature within the column was monitored using a metal thermometer (with digital display) inserted through the top of the column to a point just above the resin bed. The thermometers used during experimentation were calibrated by the SRTC Standards Laboratory.

3.3.2 Analysis Methods and Instrumentation

Simulant samples collected during the kinetics testing were submitted to the Analytical Development Section (ADS) for analysis. Analysis methods included Inductively Coupled Plasma – Mass Spectroscopy (ICP-MS), Inductively Coupled Plasma-Emission Spectroscopy (ICP-ES), Ion Chromatography-Anion (IC Anion), and Microtrac® particle size analysis. Quality assurance and control procedures and blank and standard results for each analysis set are documented and maintained by ADS and are not reported here.

Analyses not performed by ADS included density, viscosity, and chord-length determination. Liquid density measurements were conducted in duplicate by measuring the mass of a sample required to fill a 100 mL volumetric flask at ambient temperature (20 ± 2°C). Simulant viscosity measurements were also conducted in duplicate at ambient temperature (20 ± 2°C) using a Cannon-Renske Viscometer. Chord-length analyses were conducted using a Lasentec® FBRM (Focused Beam Reflectance Measurement) M400L. It should be noted that although the Lasentec® software term referring to chord-length is "square-weighted", it actually refers to a cubic or volume-type correction.

3.3.3 Supporting Equipment

Digital balances used during experimentation were calibrated by the SRTC Standards Laboratory. The calibration was checked in the laboratory prior to use each day.

3.4 Experimental Procedure

The general experimental procedure is described below. Targeted experimental variables are given in Table 3-8.

Immediately prior to each kinetics experiment an F-factor determination was performed on the appropriate resin as described in Section 3.1.2. From the same filter cup, 0.8374 ± 0.0003 g of resin was quickly weighed into the glass spacer of the differential column. Assembly of the column was completed. The SuperLig® 639 was pretreated with 120 mL 0.25 M NaOH passed upflow through the resin bed, and the resin remained covered with caustic for two hours. After

two hours the remaining caustic was removed by vacuum from the bottom of the column. Any liquid remaining in the tubing and/or pump was purged.

The appropriate simulant was filtered using a 0.45 μm Nalgene® filter cup and samples were collected for submission to ADS for ICP-MS, ICP-ES, and IC Anion analyses. The simulant was weighed into a 125 mL polyethylene bottle yielding 120 mL of feed solution. A PTFE stir bar was added, and the bottle was sealed with the modified cap.

The jacketed beaker was placed on a stir plate and attached in series to the recirculator and jacketed differential column as described above. A chiller set at 15°C was attached to the recirculator for the 25°C experiments. The recirculator was set to yield the appropriate temperature and the water flow was initiated. The simulant bottle was placed in the jacketed beaker and water was added to the beaker to simulant level. The mushroom cap was added and the argon, feed, and outlet lines were inserted. The argon and outlet lines were installed at a level above the feed line intake. Argon flow was initiated that yielded on average 2-3 mm bubbles at a flow rate of approximately 150-200 bubbles/min. Stirring was initiated within the simulant bottle and the column and the simulant were equilibrated to the experimental temperature.

Experiments using temperatures of 35°C and 45°C required the pump head to be preheated by heat tape for 5-10 minutes prior to simulant contact and continued throughout experimentation. Adjustments were continually made during these experiments to fine-tune the temperature of the simulant as it passed through the resin bed.

The pump was set to the appropriate setting as determined by the previously generated calibration curve. The pump was turned on and timing was initiated when the simulant made contact with the resin bed. Due to the extremely slow flow rates of Experiments 10 and 11, the simulant was initially passed through the system at a rapid flow rate until it reached the beginning of the outlet line. At this time the flow rate was slowed to the experimental rate and timing was initiated.

Samples were collected from the simulant bottle using a 5 mL syringe with a 4-inch #18 stainless steel needle at 15 minutes and 1-, 4-, 8-, 24-, 48-, 72-, and 120-hours. Sample volumes were 0.5 mL each, with exception of the 120-hour samples, and were submitted to ADS for ICP-MS analysis. At the completion of the experiment (120 hours) samples were collected and submitted to ADS for ICP-MS, ICP-ES, and IC Anion analyses. Weights of each sample and the temperature of the simulant at each sampling were recorded. The outlet (return) line was then removed from the simulant bottle and an effluent flow rate verification was performed using a graduated cylinder and stopwatch.

Table 3-1. F-factor values of SuperLig® 639 resin (batch I-R2-03-27-02-20-45) based on oven- and filter-dried resin masses.

Kinetics Experiment [a]	Isolation Date	Conditioning Date	Experiment Date	Particle Size [b] (μm)	F-factor
Experiment 1	04/23/02	05/24/02	08/15/02	Unsieved	0.6931
Experiments 2/3 [c]	08/23/02	08/23/02	08/27/02	Unsieved	0.7002
Experiment 4	08/23/02	08/23/02	09/10/02	Unsieved	0.6950
Experiment 5	08/23/02	08/23/02	09/10/02	850-2000	0.7136
Experiment 6	08/23/02	08/23/02	09/17/02	425-850	0.7106
Experiment 7	08/23/02	08/23/02	09/17/02	250-425	0.7034
Experiment 8	08/23/02	08/23/02	10/04/02	Unsieved	0.6926
Experiment 9	08/23/02	08/23/02	10/12/02	Unsieved	0.6911
Experiments 10/11 [d]	08/23/02	08/23/02	09/26/02	Unsieved	0.7084

[a] F-factor determination was performed immediately prior to the kinetics experiment(s) indicated. See Table 3-8 for experimental specifics.
[b] Indicated particle size is based on wet sieve analysis of conditioned resin as described in Section 3.1.3. From this same analysis, the particle size of unsieved resin was determined to be 250-2000 μm.
[c] Experiments 2 and 3 used resin from the same sub-sample of filter-dried resin. Thus, only one F-factor was performed.
[d] Experiments 10 and 11 used resin from the same sub-sample of filter-dried resin. Thus, only one F-factor was performed.

Table 3-2. Particle size distribution of conditioned SuperLig® 639 resin (batch I-R2-03-27-02-20-45) based on wet-sieve analysis.

ASTM Sieve Size	Opening (μm)	Approximate %
10	2000	0
20	850	5
40	425	93
60	250	2
325	45	0

Table 3-3. Scoping particle size distribution of conditioned SuperLig® 639 resin (batch I-R2-03-27-02-20-45) based on wet-sieve analysis.

ASTM Sieve Size	Opening (μm)	Mass %
20	850	2.25
30	600	29.28
40	425	66.41
50	300	2.07
60	250	0.00
100	150	0.00

Table 3-4. Particle size distribution comparison of conditioned SuperLig® 639 resin (batch I-R2-03-27-02-20-45) based on wet-sieve, Lasentec®, and Microtrac® analyses.

Fraction (ASTM Sieve Size)	Particle Size (μm)	Lasentec® Average Diameter [b] (μm)		Microtrac® Average Diameter [c] (μm)
		Method 1	Method 2	
Unsieved [a]	2000-250	393	441	No analyses
10-20 mesh	2000-850	667	760	No analyses
20-40 mesh	850-425	441	442	482
40-60 mesh	425-250	337	368	376

[a] The unsieved fraction is known to be 10-60 mesh since the resulting sieve fractions culminate in this range.
[b] Method 1 = mean value based on square weighting. Method 2 = mode value based on square-weighting. Incomplete analyses of the 10-20 mesh and unsieved fractions due to the 1000 μm upper detection limit.
[c] Based on mean volume distribution. Incomplete analyses of the 20-40 mesh fraction due to the 704 μm upper detection limit.

Table 3-5. Density and viscosity data for Hanford waste simulants.

Simulant	Experiment #	Density (g/mL)	Viscosity (cP)
AN-105 [a]	1-9	1.233	2.98
AZ-102	10	1.232	3.05
AN-107	11	1.258	3.37

[a] The same batch of simulant was used for Experiments 1-9 and the density and viscosity were determined from the bulk simulant, not for each experiment.

Table 3-6. Expected concentrations of selected species in original Hanford simulants based on reagents added.

Species	AN-105 (M)	AZ-102 (M)	AN-107 [a] (M)
Na	5.000	5.000	5.000
K	0.090	0.153	0.027
Al	0.687	0.053	0.008
S	0.004	0.325	0.051
P	0.003	0.009	0.007
Cr	0.012	0.037	0.000 [c]
Mg	1.04E-04	6.94E-05	6.07E-04
Ca	4.66E-04	5.08E-03	1.59E-03
Sr	0.000 [b]	4.34E-06	4.46E-05
Ba	0.000 [b]	1.08E-05	3.20E-05
Cd	1.37E-05	3.26E-05	0.000 [c]
B	2.21E-03	1.08E-05	1.91E-03
Si	3.51E-03	3.75E-02	0.000 [b]
Mn	0.000 [b]	6.94E-05	6.01E-03
Fe	0.000 [b]	3.79E-04	1.79E-02
Ni	0.000 [b]	6.94E-05	5.32E-03
Mo	4.00E-04	1.14E-03	2.20E-04
Pb	1.20E-04	5.43E-05	0.000 [c]
Nitrate	1.243	0.515	2.188
Nitrite	1.126	1.243	0.784
Sulfate	0.004	0.325	0.051
Phosphate	0.003	0.009	0.007
Chloride	0.120	0.013	0.030
Fluoride	0.005	0.101	0.004
Oxalate	3.24E-03	0.061	0.006
Formate	2.99E-02	0.000 [b]	0.136
Added Hydroxide	1.60	0.206	0.012
Carbonate	0.098	0.964	0.825
TIC	0.098	0.964	0.825
TOC	0.140	0.949	1.981

[a] Significantly altered from the original composition during strontium/ transuranics precipitation testing.
[b] Species absent from the Eibling recipe and not added to simulant.
[c] Species included in the Eibling recipe but not added to simulant.

Table 3-7. Average molar concentrations of selected species in Hanford simulants used in kinetics testing as measured by ICP-ES and ion chromatography.

Species	AN-105 Experiment # 1-9	AZ-102 Experiment # 10	AN-107 Experiment # 11
Na	4.988	4.937	5.676 [a]
K	0.095	0.150	0.034
Al	0.598	0.049	0.009
S	0.004	0.320	0.054
P	0.003	0.010	0.010
Cr	0.012	0.026	<9.62E-06
Mg	<3.17E-05	<3.46E-05	<3.46E-05
Ca	9.21E-06	1.67E-03	3.48E-03
Sr	<6.00E-07	6.73E-06	1.00E-03 [a]
Ba	3.75E-06	2.15E-06	<1.46E-06
Cd	1.23E-05	<1.25E-06	<1.25E-06
B	2.62E-03	7.68E-04	1.91E-03
Si	3.61E-03	<4.63E-05	3.33E-04
Mn	1.50E-06	<1.64E-06	9.46E-06 [b]
Fe	7.45E-05	<8.95E-06	3.03E-04 [b]
Ni	<1.02E-05	<1.06E-05	5.40E-03
Mo	4.04E-04	1.10E-03	2.22E-04
Pb	1.15E-04	<3.33E-05	<3.33E-05
Re	7.76E-05	2.00E-04	2.98E-05
Nitrate	1.077	0.442	2.209 [a]
Nitrite	1.096	1.137	0.780
Sulfate	0.003	0.276	0.049
Phosphate	0.002	0.011	0.017
Chloride	0.105	<5.64E-04	0.035
Fluoride	0.001	0.133	0.088
Oxalate	0.002	0.016	0.012
Formate	0.036	0.174	0.131

[a] Indicates species whose concentrations were expected to increase due to precipitation processing.
[b] Indicates species whose concentrations were expected to decrease due to precipitation processing.

Table 3-8. Targeted experimental variables for kinetics testing using SuperLig® 639 resin (batch I-R2-03-27-02-20-45).

Kinetics Experiment [a]	Start Date	Sieve Cut	Temperature	Flow Rate (mL/min)	Simulant
Experiment 1	08/15/02	Unsieved	25°C	30	AN-105
Experiment 2	08/27/02	Unsieved	25°C	30	AN-105
Experiment 3	08/27/02	Unsieved	35°C	30	AN-105
Experiment 4	09/10/02	Unsieved	45°C	30	AN-105
Experiment 5	09/10/02	10-20 mesh	25°C	30	AN-105
Experiment 6	09/17/02	20-40 mesh	25°C	30	AN-105
Experiment 7	09/17/02	40-60 mesh	25°C	30	AN-105
Experiment 8	10/04/02	Unsieved	25°C	1	AN-105
Experiment 9	10/12/02	Unsieved	25°C	0.5	AN-105
Experiment 10	09/26/02	Unsieved	25°C	30	AZ-102
Experiment 11	09/26/02	Unsieved	25°C	30	AN-107

[a] Experiment 1 used resin isolated 04/23/02 and conditioned 05/24/02. All other experiments used resin isolated 08/23/02 and conditioned 08/23/02.

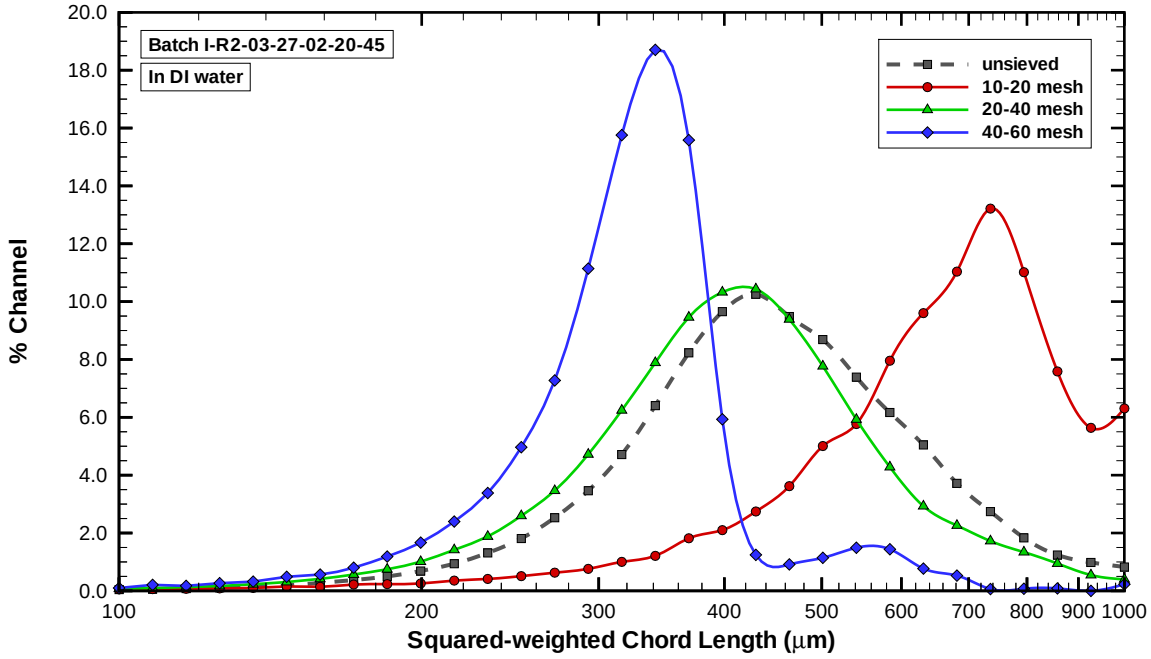

Figure 3-1. Particle size (chord length) distributions of sieve fractions and unsieved SuperLig® 639 as measured using Lasentec® analyses.

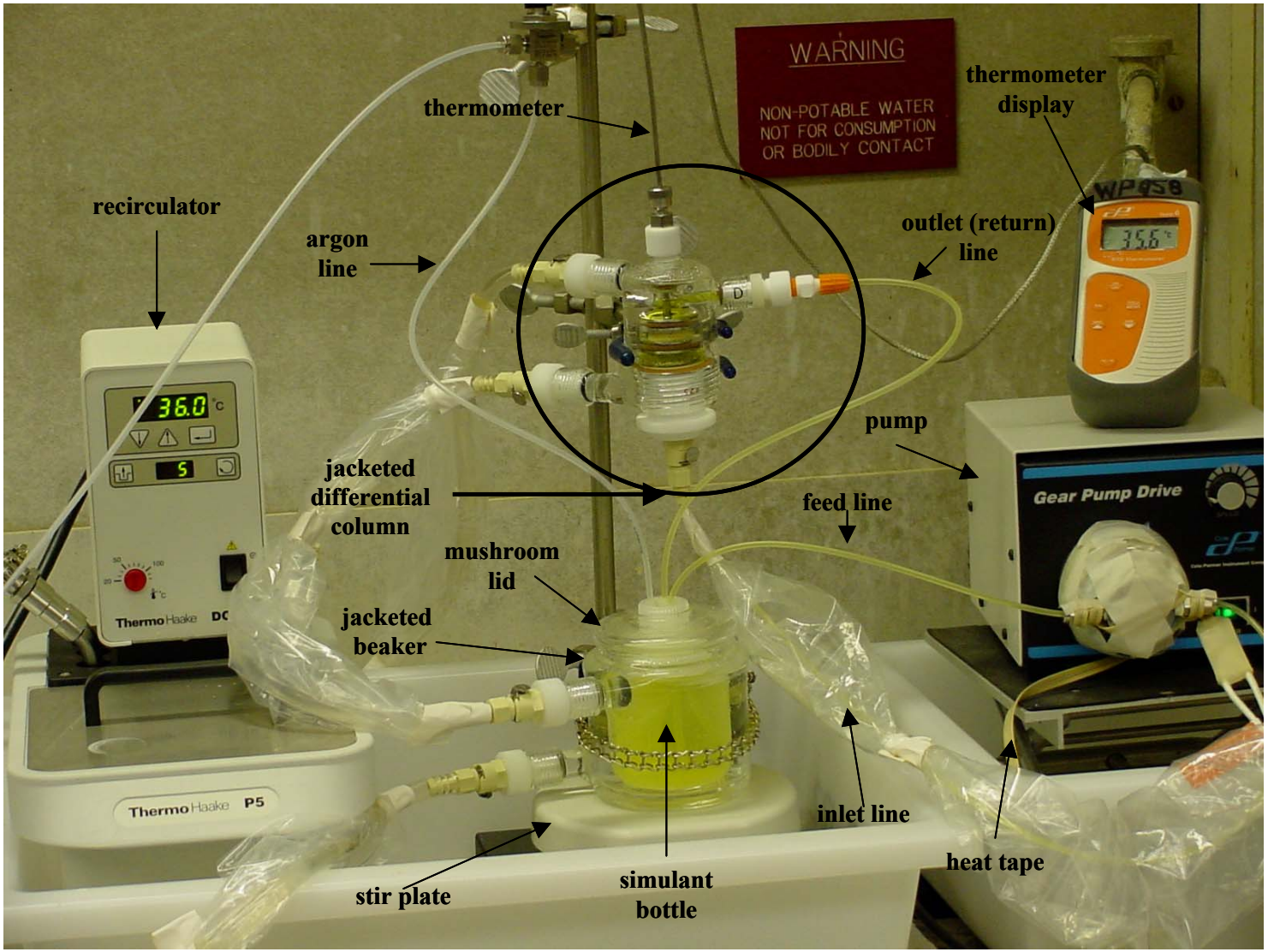

Figure 3-2. Photograph of complete kinetics experimental setup during operation.

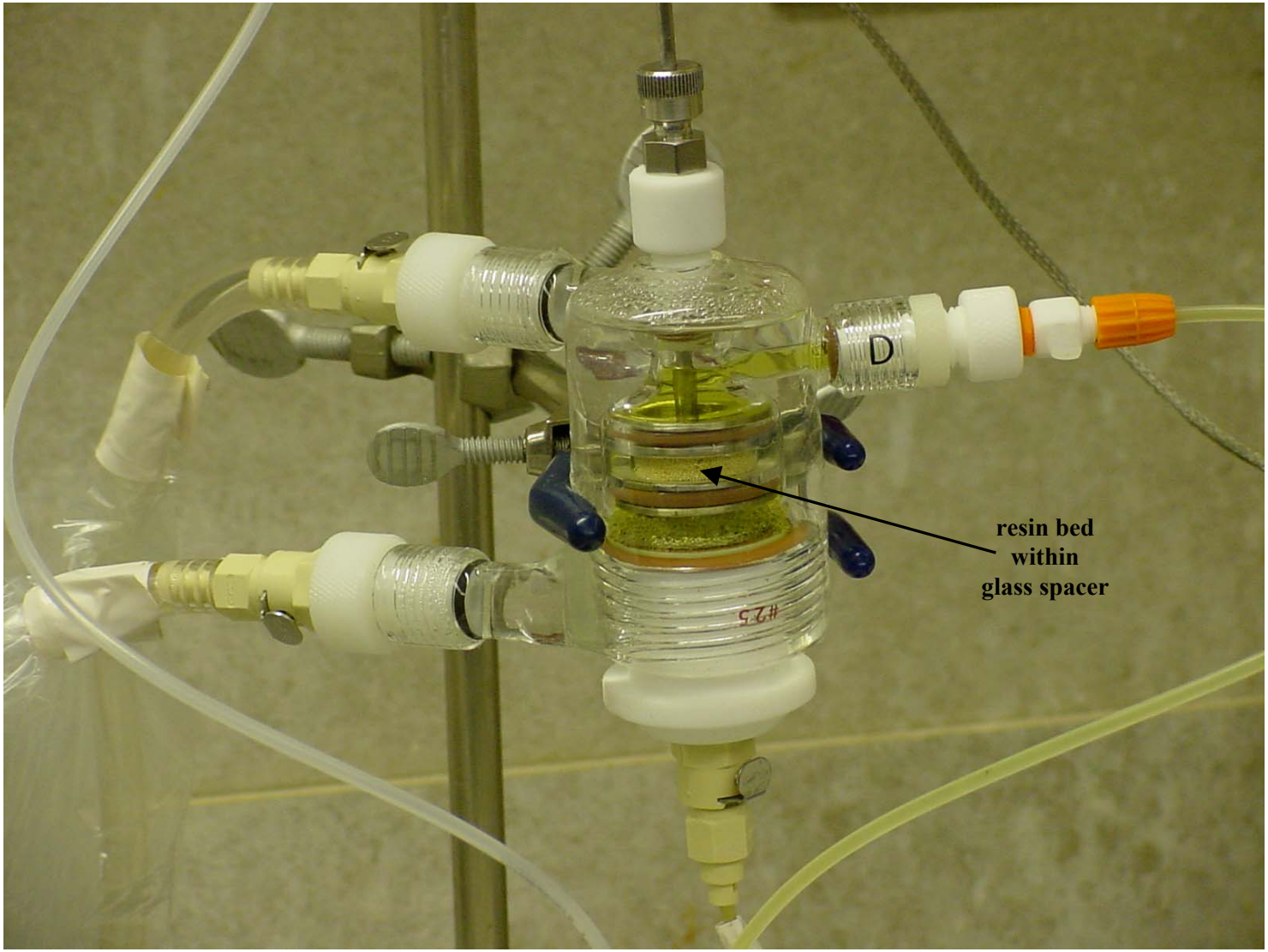

Figure 3-3. Photograph of differential column during operation.

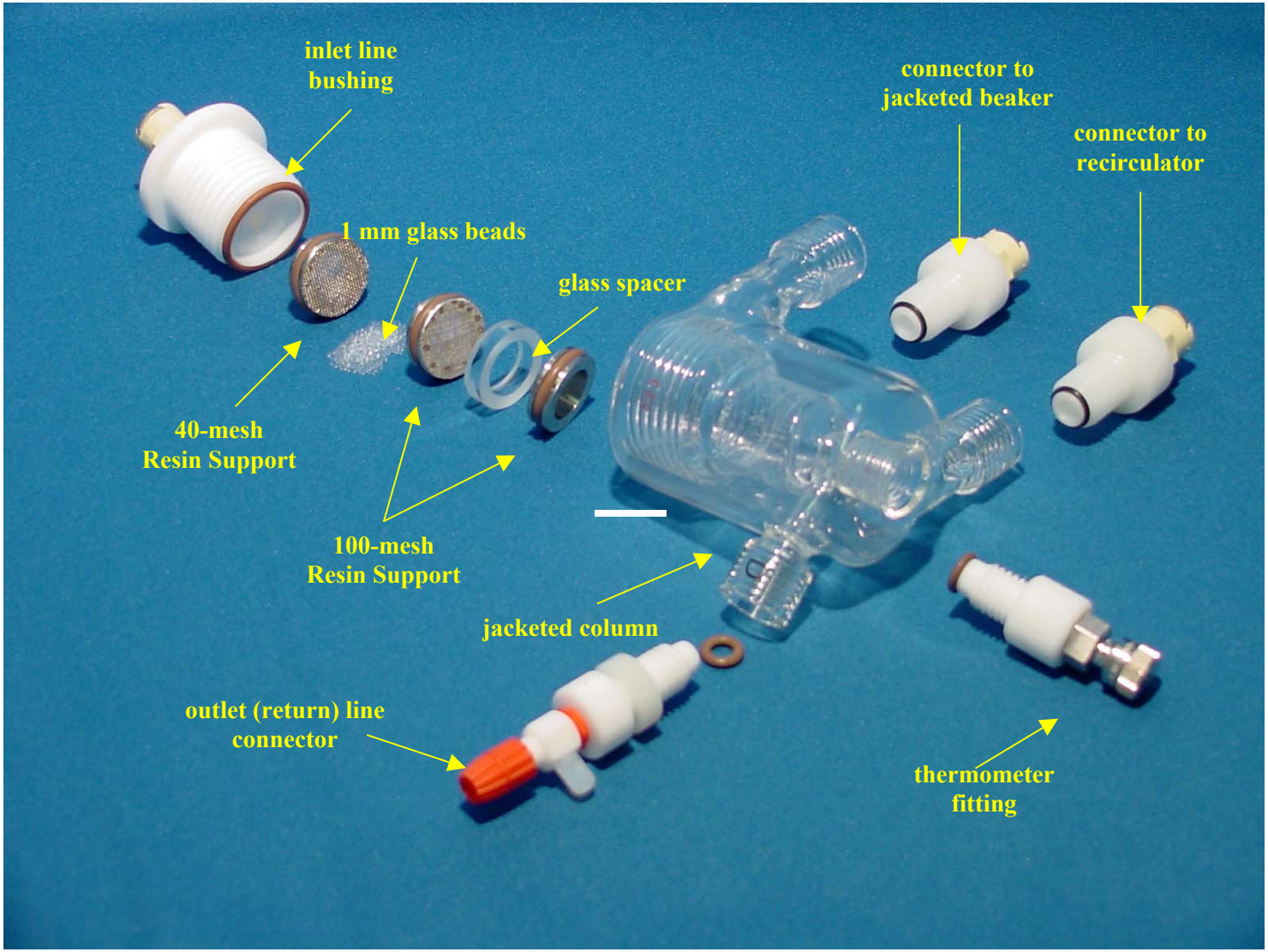

Figure 3-4. Photograph of exploded view of differential column.

4.0 Results and Discussion

In this chapter the results for the kinetics and equilibrium adsorption behavior of rhenium (in its perrhenate form) onto SuperLig® 639 resin particles are presented. One of the main objectives of this work was the creation of a complete kinetics data set that would provide a technical basis for determining key resin properties (i.e., modeling parameters) to be used in the IX column modeling efforts based on the VERSE-LC code. The basic overall test matrix was designed to address the impact of:

- temperature on particle kinetics and adsorption capacity (based on discussions with the manufacturer of SuperLig® 639 resin, IBC, and earlier elution studies, it was anticipated that the adsorption capacity would be strongly dependent upon temperature);
- average particle size on particle kinetics and adsorption capacity (based on discussions with the manufacturer of SuperLig® 639 resin, IBC, it was anticipated that the adsorption capacity would not be particle size dependent);
- flow rate through the differential column on overall particle kinetics (here the first objective was to determine an acceptable upper bound flow rate where the film mass transfer resistance at the outer particle surface would be negligible and the second objective was to estimate the superficial velocity dependence on the film coefficient); and
- liquid-phase composition upon the particle kinetics and adsorption capacity (simulant composition effects will impact the migration rates of species (e.g., resulting from changes in fluid viscosity) and the isotherms (e.g., resulting from ionic competitors and enhancers)).

In the subsections to follow, for the four topics mentioned above, the results from a series of kinetics experiments are presented. In the fifth subsection the equilibrium results are compared with previous batch contact test data (King et al., 2000 and Hassan et al., 2000) and the preliminary isotherm model by Hamm et al. (2000b).

In total, eleven kinetics experiments were performed. To reduce the total number of separate kinetics experiments required, a nominal set of testing conditions was chosen about which additional testing was performed by varying the key parameters outlined above. The nominal testing conditions correspond to those used in Experiments 1 and 2, as defined below. For consistency, all testing was performed using the same batch of SuperLig® 639 resin (batch I-R2-03-27-02-20-45) received April 2002. Experiment 1 was the only test performed using resin that was isolated 04/23/02 and conditioned 05/24/02. All other testing (i.e., Experiments 2 – 11) used resin from the same sample isolated 08/23/02 and conditioned on that same date. Comparisons made to nominal testing conditions used results from Experiment 2. With exception of the test series varying flow rate, a high value of flow rate (i.e., 30 mL/min (12.5 cm/min)) was chosen such that the mass transfer resistance associated with surface film diffusion can be considered small. All kinetic experiments were performed with an initial phase ratio greater than 200 in an attempt to minimize the impacts associated with the eight sampling withdrawals, each sample withdrawal being ~0.5 mL). Each kinetics test was operated with a total of 120 hours of simulant contact time. During the 5-day contact period, samples were

withdrawn at the approximate time points: 0.25, 1, 4, 8, 24, 48, 72, and 120 hours. All sample concentrations (including feed concentrations) were analyzed using ICP-MS. All concentrations listed in Tables 4-1 through 4-8 were obtained using ICP-MS unless otherwise indicated. Feed concentrations and 120-hour sample concentrations were also analyzed using ICP-ES and IC Anion methods. These results are listed in Appendices A-K. The total experiment duration and selected sampling times were based on pre-test VERSE-LC simulations where the preliminary SuperLig® 639 models (Hamm et al., 2000b) were used. The early sampling times provide key information about the pore diffusion process, while the later sampling times provide information on the true equilibrium state (as discussed in Section 2.2). The measured Re concentrations, along with key testing conditions, are provided for each test where the transient Re K_d value $[K_d(t)]$, the transient Re loading level [Q(t)], and the transient normalized Re concentration $[\eta(t)]$ were computed using Eqs. (2-9), (2-10), and (2-11), respectively.

For comparison purposes, graphs showing the transient Re loading levels and normalized Re concentrations have been chosen. To better illustrate the early on kinetics aspect of each test, the graphs showing the normalized Re concentrations are shown in semi-log scale.

4.1 Temperature Dependency of Perrhenate Adsorption Kinetics

To study the impact of contact temperature on the particle kinetics and equilibrium adsorption capacity, four separate kinetics experiments were performed (i.e., Experiments 1 – 4). The specific conditions of each temperature dependent kinetics test are listed in Table 4-1. Testing was performed at 25, 35, and 45ºC using the standard Envelope A (AN-105) simulant. Based on previous variability associated with measured K_d values obtained from traditional batch contact testing, initial testing of the kinetic experimental setup focused on this. Experiment 2 was a repeat of Experiment 1 to establish the level of reproducibility given by the kinetics test apparatus and testing methodology. For the four experiments listed in Table 4-1, the measured liquid-phase Re concentrations at the selected sampling times are given in Table 4-2. Table 4-2 also provides the measured initial liquid-phase Re concentrations, as well as the computed Re loading and K_d values.

The computed Re loading and normalized concentration levels for each temperature dependent test are plotted in Figures 4-1 and 4-2, respectively. As shown in Figure 4-1, reasonably good reproducibility can be achieved with this kinetics test apparatus operating under the testing protocols employed. As expected and shown in Figure 4-1, the adsorption capacity of SuperLig® 639 resin (i.e., the plateau regions at late contact times) drops at higher temperatures. A drop in capacity of approximately 1.5% is observed for every 1ºC increase in contact temperature. Also, the results shown in Figure 4-1 indicate that no appreciable resin degradation (or slower competitor) effects are occurring over the 120 hour contact period as no decrease in capacity is observed. This indicates that a "true" equilibrium point on the appropriate adsorption isotherm has been measured.

A simulant's dynamic viscosity can play a major role in determining the value of a species "free-stream" (i.e., molecular) diffusion coefficient. A species "free-stream" diffusion coefficient goes up with increasing temperature based on the Stokes-Einstein equation discussed in Hamm et al.

(2000b). Given this trend one would expect, based on Eq. (2-12), that particle kinetics would be faster for higher temperatures since the tortousity factor should be somewhat temperature independent. When looking at the normalized Re concentration curves shown in Figure 4-2, this basic trend can be seen (i.e., at higher temperatures the curves shift to higher levels at the same points in time).

4.2 Particle Size Dependency of Perrhenate Adsorption Kinetics

To study the impact of particle diameter on the particle kinetics and equilibrium adsorption capacity, three additional kinetics experiments were performed (i.e., Experiments 5 – 7) using three sieve fractions of the SuperLig® 639 resin. The test conditions chosen were consistent with those of Experiment 2, with the exception of the variation in particle size. In this way, results from Experiment 2 would provide a basic comparison of the composite behavior of the unsieved material. Based on prior information from IBC it was anticipated that the adsorption capacity (in units of mmol of Re adsorbed/g of dry resin) of SuperLig® 639 particles would not be a function of particle diameter. In addition, it was expected that slower adsorption rates would be observed for particles of larger diameter. This expectation is consistent with the notion that the active adsorption sites are uniformly distributed throughout the pore structure of each particle.

A sample of conditioned SuperLig® 639 resin was sieved into three fractions (10-20 mesh, 20-40 mesh, and 40-60 mesh) as described in Section 3.1.3. The resulting average particle diameter for each sieve fraction was 760 μm, 442 μm, and 368 μm, respectively (Lasentec® analysis mode value based on square-weighting). The average particle diameter for the unsieved resin was 441 μm based on the same analysis method. The composite of the three sieve fractions included all particle sizes contained within the unsieved material used in Experiment 2. Section 3.1.3 provides further details of the particle size distribution.

The specific conditions of each particle size dependent kinetics test are listed in Table 4-3. Testing was performed with 10-20 mesh, 20-40 mesh, and 40-60 mesh SuperLig® 639 sieve fractions and the standard Envelope A (AN-105) simulant. For the experiments listed in Table 4-3, the measured liquid-phase Re concentrations at the selected sampling times are given in Table 4-4. Table 4-4 also provides the initial liquid-phase Re concentrations, as well as the computed Re loading and K_d values.

The computed Re loading and normalized concentration levels for each particle size dependent test are plotted in Figures 4-3 and 4-4, respectively. As expected and shown in Figure 4-3, the adsorption capacity of SuperLig® 639 (i.e., the plateau regions at late contact times) is particle size independent.

Under different testing conditions where the species “free-stream” diffusion coefficients are maintained constant and only the average particle diameter is allowed to increase, it was expected that the rate of particle kinetics would drop. This assumes that the tortousity factor for the material is not particle size dependent; therefore, the pore diffusion coefficients (as given by Eq. (2-12)) would remain approximately constant. When looking at the normalized Re

concentration curves shown in Figure 4-4, this basic trend can be seen (i.e., at higher average particle diameters the curves shift to lower levels at the same points in time). Note that the data point at the sampling time of 4 hours in Experiment 5 is considered to be an outlier.

At equilibrium the mass average loading value of Experiments 5 – 7 (the three sieve fractions) should be equivalent to the measured loading level of Experiment 2 (the unsieved resin). The transient Re loading and normalized concentration levels for all four tests are provided for comparison in Figures 4-5 and 4-6, respectively. As shown in Figure 4-5, a systematic bias in loading capacity exists between the average behavior of the three sieve fraction tests and the unsieved test at the late contact times. The equilibrium loading performance of the three sieve fraction tests are internally consistent; however, their common value falls below the unsieved resin test result. Later kinetics testing (Experiments 8 and 9) under similar conditions (i.e., at 25ºC and with AN-105 simulant), indicated that the apparent reduction in measured Re loading levels was limited to only those resin samples that were sieved. In Figure 4-7 the kinetics results for all kinetics testing at 25ºC and with AN-105 simulant are plotted for direct comparison. As shown in Figure 4-7, an approximately 8% reduction is observed for the sieved resin samples. One possible reason for this might be degradation to the outer surfaces of the particles due to mechanical actions associated with the sieving process. Alternatively, air entrapment within the pore structure during the sieving process may have led to a reduced "effective" capacity for the sieve fractions (see Section 3.1.3). The observed floating of the resin particles in the sieve fractions indicated the air entertainment had occurred during the wet-sieving process.

At very short time periods the diffusional process is limited to just the outer surface regions of each resin particle (i.e., both large and small diameter particles). Given this, the kinetics aspects of a population of varying size particles should follow more closely with the kinetic behavior of the smaller diameter particles. At much longer points in time where the entire population is approaching equilibrium, the kinetics aspects will shift toward the kinetic behavior of the larger particles (i.e., longer diffusional path-lengths). Ultimately, once complete equilibrium is obtained, the observed loading levels for differing sizes of particles sets (here sieve fractions) should be consistent with the mass average loading level of their composite.

In Figure 4-6, at early times the particle kinetics behavior for the unsieved Experiment 2 test falls slightly under the results for the small diameter sieve fraction (40-60 mesh) and then appears to be shifting towards the larger particle sieve fraction (10-20 mesh) at later times. This kinetics behavior shift from the small towards the large particle behavior is consistent with expectations.

4.3 Flow Rate Dependency of Perrhenate Adsorption Kinetics

As mentioned earlier, the observed overall kinetics is established based primarily on the net result of mass transfer limitations at the particle level. Specifically, the overall mass transfer mechanisms of interest are: (1) film diffusion across the stagnant layer of liquid surrounding each individual particle, and (2) species molecular diffusion through the particle's pore structure. The particle's pore diffusion coefficients can be isolated for indirect measurement by increasing the rate of film diffusion based on increased liquid flow rate about the particles. Basically, the film diffusion coefficient has a functional dependence expressed as:

$$k_f = F(u_o) \tag{4-1}$$

where k_f - film diffusion coefficient (cm/min)
u_o - superficial velocity through bed (cm/min)

As discussed in Hamm et al. (2000b), for the SuperLig® 639 resin beds the Wilson and Geankoplis (1966) correlation was chosen. This correlation was chosen primarily due to its range of Reynolds Number spanning the range of expected SuperLig® 639 column operations. To date no kinetics data has been available to verify or upgrade the VERSE-LC column modeling methodology. By varying the flow rate imposed on the differential column, the kinetics apparatus used in this study has the capability to provide such a database.

As indicated earlier, Experiment 2 represents the nominal testing conditions. The flow rate for this experiment was 30 mL/min (i.e., a superficial velocity through the differential bed of ~12.5 cm/min). Initial scoping tests using SuperLig® 644 and flow rates of 30, 60, and 90 mL/min confirmed that a 30 mL/min flow rate results in sufficiently high film mass transfer rates. This was further confirmed through VERSE-LC simulations, where flow rates above this value had only minor shifts in the predicted transient Re concentration levels.

To provide additional kinetics data for either confirming or upgrading the Wilson and Geankoplis (1966) correlation, two additional separate kinetics experiments were performed (i.e., Experiments 8 and 9) where the flow rate (i.e., superficial velocity) was lowered such that the mass transfer resistance associated with film diffusion was no longer negligible. The targeted values of the lower flow rates were established based on pre-test prediction made using the VERSE-LC code and its preliminary methodology as stated in Hamm et al. (2000b). Again, the test conditions were chosen consistent with those for Experiment 2. In this way, Experiment 2 results provide a direct comparison of the impact that film diffusion has on the overall particle kinetics.

The specific conditions of each flow rate dependent kinetics test are listed in Table 4-5. Testing was performed at flow rates of 1 mL/min (0.416 cm/min) and 0.5 mL/min (0.208 cm/min) using the standard Envelope A (AN-105) simulant. For the experiments listed in Table 4-5, the measured liquid-phase Re concentrations at the selected sampling times are given in Table 4-6.

Table 4-6 also provides the initial liquid-phase Re concentrations, as well as the computed Re loading and K_d values.

The computed Re loading and normalized concentration levels for each flow rate dependent test are plotted in Figures 4-8 and 4-9, respectively. As expected and shown in Figure 4-7, the adsorption capacity of SuperLig® 639 is independent of flow rate. Only the time required to reach a true equilibrium value varies. Note that Experiments 2, 8, and 9 represent three independent resin loadings (i.e., a different resin bed was used for each flow rate test). Again the results shown in Figure 4-7 indicate that good reproducibility of the equilibrium state can be achieved when using this kinetics experimental setup.

The impact of decreasing the flow rate is best illustrated by the normalized Re concentration curves shown in Figure 4-9. At the lowest flow rate (i.e., 0.5 mL/min in Experiment 9) the transport lag time associated with the connecting tubing within the kinetics apparatus is also clearly noted. To adequately interpret the functional dependence of the superficial velocity on the film coefficient (i.e., Eq. (4-1)), the transport time delays must also be accounted for during data analysis.

4.4 Simulant Dependency of Perrhenate Adsorption Kinetics

To study the impact of solution composition on the particle kinetics and equilibrium adsorption capacity, two additional kinetics experiments were performed (i.e., Experiments 10 and 11). The test conditions chosen were consistent with those from Experiment 2 with the exception of simulant composition. The specific conditions of each simulant dependent kinetics test are listed in Table 4-7. Testing was performed using Envelope B (AZ-102) and Envelope C (AN-107) simulants (see Section 3.2 for simulant details). For the experiments listed in Table 4-7, the measured liquid-phase Re concentrations at the selected sampling times are given in Table 4-8. Table 4-8 also provides the initial liquid-phase Re concentrations, as well as the computed Re loading and K_d values. The computed Re loading and normalized concentration levels for each simulant dependent test are plotted in Figures 4-10 and 4-11, respectively.

Based on prior information about the adsorption isotherm (see Hamm et al., 2000b), nitrate is the predominate competitor for perrhenate. The true equilibrium loading levels will depend strongly on the nitrate to perrhenate molar ratio. For the three simulants tested, the approximate nitrate to perrhenate ratios are listed in Table 4-9. Based on more recent elution analyses performed by King et al. (2002), it is now believed that the SuperLig® 639 resin has a much higher adsorption affinity for the potassium salt ($KReO_4$) versus the sodium salt ($NaReO_4$). As such, the perrhenate isotherm is also impacted by the sodium to potassium molar ratio. The approximate sodium to potassium molar ratios for the three simulants tested are also provided in Table 4-9.

Based on this wide range in nitrate-to-perrhenate ratios and the understanding of the perrhenate isotherm (see Section 2.2), it was expected that loading levels at equilibrium would vary inversely with this ratio. As expected and shown in Figure 4-10, the adsorption capacity of SuperLig® 639 varies inversely with the nitrate-to-perrhenate ratio, and decreases in the order Envelope B (AZ-102), Envelope A (AN-105), and Envelope C (AN-107). At later contact times

the loading levels for Envelopes A and B reach a plateau indicating that a true equilibrium value has been reached where potential degradation or slower competitor effects were not observed. A slight decrease in loading was observed for the Envelope C simulant samples taken at 72 and 120 hours. This is thought to be a sensitivity issue with the ICP-MS analyses (due to organic constituents) rather than degradation or slower competitor effects. For confirmation the Envelope C samples were analyzed using ICP-ES analyses wherein this loading decrease was not observed, again indicating that a true equilibrium value has been reached. Note that the data point at the sampling time of 48 hours is considered to be an outlier. A comparison of the ICP-MS and ICP-ES analyses showing the computed Re loading and normalized concentration levels for the Envelope C test are plotted in Figures 4-12 and 4-13, respectively.

As mentioned under the section discussing the temperature variation impacts, a simulant's dynamic viscosity can play a direct role in determining the value of a species pore diffusion coefficient. Based on the Stokes-Einstein equation discussed in Hamm et al. (2000b), a species pore diffusion coefficient is expected to go up with decreasing fluid viscosity. Given this trend one would expect based on Eq. (2-12), that particle kinetics would be faster for lower viscosity simulants since the tortousity factor should be somewhat simulant independent. The normalized Re concentration curves shown in Figure 4-11, indicate a basic trend opposite to that expected (i.e., at higher viscosities the curves shift to higher levels at the same points in time, see Table 3-5 for measured simulant viscosities). Unfortunately, other compositional factors can impact the kinetics behavior and perhaps these effects are significant enough to actually reverse the viscosity impact.

4.5 Perrhenate Adsorption Isotherm

In the results discussed so far, focus has been predominantly on the transient behavior of SuperLig® 639 particles. However, it has also been pointed out that for the majority of kinetics experiments performed a "true" equilibrium state was achieved by the last sampling time (i.e., 120 hours). The basis for this, centers around the observed loading level plateaus experienced prior to reaching the 120-hour sampling time. From these various experiments we also can see a clear impact on perrhenate loadings due to contact temperature and liquid-phase composition (i.e., particularly with respect to the nitrate to perrhenate molar ratio).

As discussed earlier in Section 2.2, the basic equilibrium adsorption chemistry for SuperLig® 639 resins in contact with the simulants of interest can be expressed in the form of a simple algebraic isotherm model (i.e., see Eq. (2-6)). As indicated in Eq. (2-6), once the two resin specific parameters (i.e., the total perrhenate loading capacity ($\overline{C}_T$) and nittrate-to-perrhenate selectivity coefficient ($\widetilde{K}_{21}$)) have been determined, a modest range of predictable equilibrium adsorption behavior can be estimated. Based on discussions with the manufacturer (IBC) of SuperLig® 639 resins, it can be assumed that the nitrate-to-perrhenate selectivity coefficient is only temperature dependent, while the total perrhenate loading capacity is batch specific with a temperature and liquid-phase compositional dependency (see Section 2.2).

Based on earlier batch contact testing, Hamm et al. (2000b) estimated these two parameters for a batch of SuperLig® 639 resin made in 1998 (i.e., id = 981015DHC720011). The batch contact

testing that was performed (i.e., King et al. (2000) and Hassan et al. (2000)), measured the perrhenate loading levels after a 24 hour shaker table contacting period at 25ºC. An Envelope A simulant was chosen consistent with Tank AN-105. The estimate values for these two parameters were:

- $\overline{C}_T = 0.6472$ ($mmol_{ReO4}/g_{resin}$)
- $\widetilde{K}_{21} = 1.363x10^{-3}$ (-)

where under 5 M sodium conditions tested the nitrate and potassium concentration levels were 1.24 M and 0.1 M, respectively. A comparison of the algebraic isotherm model and the database used in determining the above parameters is shown in Figure 4-14. As illustrated in Figure 4-14, the isotherm model can reasonably predict the perrhenate loading levels over the wide range of nitrate-to-perrhenate ratios tested. The estimated parameters are specific to AN-105 simulant in contact with batch 981015DHC720011 where the simulant had a 5 M sodium concentration and was at 25ºC. Unfortunately, prior to 2002 the majority of batch contact testing performed was done only at a 24 hour contact period. Therefore, it is expected that these measured loading levels are not true equilibrium values and are slightly low.

For a further comparison in Figure 4-14, the kinetics results taken at the 24-hour sampling time are also plotted for the 25ºC Envelope A, B, and C simulants tested. Unfortunately, a completely consistent comparison between the various data sets shown is not possible since the batch id's, sodium levels, and potassium levels are different. At this time the algebraic isotherm model does not readily accommodate these various factors, but efforts are underway to update and reflect these observations in a future isotherm model. Looking only at the 24-hour contact data, the observed deviations for the three simulants tested in this report, about the isotherm model shown in Figure 4-14, appear consistent with the variations in total concentration of sodium plus potassium of each simulant as listed in Table 4-9. Basically, higher total cation concentration resulted in higher measured perrhenate loading levels.

However, when the 120-hour sampling time data are compared to the original isotherm model (based on previous 24-hour contact data), we see a mixture of changes occurring. As shown in Figure 4-15, the Envelope A and B data points are shifting to the right, consistent with continually approaching their true equilibrium state along their operating line. For the Envelope C simulant the data based on the ICP-MS measurement technique shifts back towards the left along its operating line. However, as discussed in Section 4.4, this is thought to be a sensitivity issue with the ICP-MS analyses (due to organic constituents). The data based on the ICP-ES measurement technique indicates a shift back in the direction to the right. It is difficult to ascertain at this time the precise amount of increased perrehnate loadings that can be attributed to a higher total ligand capacity for the new resin batch versus the increased contact times.

Table 4-1. Experimental variables for temperature dependent kinetics testing.

Variable		Experiment 1	Experiment 2	Experiment 3	Experiment 4
Start Date		08/15/02	08/27/02	08/27/02	0910/02
Simulant		AN-105	AN-105	AN-105	AN-105
Avg. Temperature (°C)		23.8	24.7	33.3	45.2
Sieve Fraction		Unsieved	Unsieved	Unsieved	Unsieved
Resin Dry Wt. (g)		0.5803	0.5834	0.5836	0.5821
Feed Volume (mL)		120	120	120	120
Phase Ratio (ϕ)		207	206	206	206
c_i (Re)	**(μg/L)**	1.39E+04	1.44E+04	1.44E+04	1.46E+04
	(M)	7.46E-05	7.73E-05	7.73E-05	7.84E-05
Flow Rate	**(mL/min)**	30	30	30	30
	(BV/hr)	1385	1385	1385	1385
	(cm/min)	12.5	12.5	12.5	12.5

Table 4-2. Results summary for temperature dependent kinetics testing.

Experiment (T)	Time, t (hr)	Liquid Re Concentration (c_f)		Loading, Q (mmol Re/g resin)	K_d (mL/g)
		(μg/L)	(M)		
Experiment 1 (25°C)	0.00	1.39E+04	7.46E-05	0.00E+00	---
	0.25	1.14E+04	6.12E-05	2.78E-03	45
	1.00	9.51E+03	5.11E-05	4.88E-03	95
	4.00	7.12E+03	3.82E-05	7.53E-03	197
	8.00	5.98E+03	3.21E-05	8.80E-03	274
	24.00	4.65E+03	2.50E-05	1.03E-02	411
	48.03	4.15E+03	2.23E-05	1.08E-02	486
	72.00	3.98E+03	2.14E-05	1.10E-02	515
	120.00	3.94E+03	2.12E-05	1.11E-02	523
Experiment 2 (25°C)	0.00	1.44E+04	7.73E-05	0.00E+00	---
	0.25	1.19E+04	6.39E-05	2.71E-03	43
	1.00	9.58E+03	5.14E-05	5.27E-03	103
	4.02	7.35E+03	3.95E-05	7.73E-03	197
	8.00	6.25E+03	3.36E-05	8.95E-03	268
	24.48	4.84E+03	2.60E-05	1.05E-02	406
	49.62	4.32E+03	2.32E-05	1.11E-02	480
	72.23	4.20E+03	2.26E-05	1.12E-02	500
	120.15	4.13E+03	2.22E-05	1.13E-02	511
Experiment 3 (35°C)	0.00	1.44E+04	7.73E-05	0.00E+00	---
	0.25	1.16E+04	6.23E-05	3.04E-03	50
	1.00	9.44E+03	5.07E-05	5.42E-03	108
	4.00	7.62E+03	4.09E-05	7.43E-03	183
	8.00	6.69E+03	3.59E-05	8.46E-03	237
	24.13	5.70E+03	3.06E-05	9.55E-03	314
	49.50	5.53E+03	2.97E-05	9.74E-03	330
	71.93	5.36E+03	2.88E-05	9.93E-03	347
	119.87	5.32E+03	2.86E-05	9.97E-03	351
Experiment 4 (45°C)	0.00	1.46E+04	7.84E-05	0.00E+00	---
	0.25	1.23E+04	6.61E-05	2.49E-03	39
	1.00	1.05E+04	5.64E-05	4.48E-03	80
	4.00	8.76E+03	4.70E-05	6.41E-03	137
	8.00	7.93E+03	4.26E-05	7.33E-03	173
	24.00	7.39E+03	3.97E-05	7.93E-03	201
	48.00	7.49E+03	4.02E-05	7.82E-03	196
	75.22	7.45E+03	4.00E-05	7.86E-03	198
	120.00	7.37E+03	3.96E-05	7.95E-03	202

Table 4-3. Experimental variables for particle size dependent kinetics testing.

Variable		Experiment 2	Experiment 5	Experiment 6	Experiment 7
Start Date		08/27/02	09/10/02	09/17/02	09/17/02
Simulant		AN-105	AN-105	AN-105	AN-105
Avg. Temperature (°C)		24.7	24.9	25.0	24.8
Sieve Fraction		Unsieved	10-20 mesh	20-40 mesh	40-60 mesh
Resin Dry Wt. (g)		0.5834	0.5979	0.5950	0.5889
Feed Volume (mL)		120	120	120	120
Phase Ratio (ϕ)		206	201	202	204
c_i (Re)	**(μg/L)**	1.44E+04	1.46E+04	1.37E+04	1.37E+04
	(M)	7.73E-05	7.84E-05	7.36E-05	7.36E-05
Flow Rate	**(mL/min)**	30	30	30	30
	(BV/hr)	1385	1385	1385	1385
	(cm/min)	12.5	12.5	12.5	12.5

Table 4-4. Results summary for particle size dependent kinetics testing.

Experiment (Sieve Fraction)	Time, t (hr)	Liquid Re Concentration (c_f)		Loading, Q (mmol Re/g resin)	K_d (mL/g)
		(μg/L)	(M)		
Experiment 2 (Unsieved)	0.00	1.44E+04	7.73E-05	0.00E+00	---
	0.25	1.19E+04	6.39E-05	2.71E-03	43
	1.00	9.58E+03	5.14E-05	5.27E-03	103
	4.02	7.35E+03	3.95E-05	7.73E-03	197
	8.00	6.25E+03	3.36E-05	8.95E-03	268
	24.48	4.84E+03	2.60E-05	1.05E-02	406
	49.62	4.32E+03	2.32E-05	1.11E-02	480
	72.23	4.20E+03	2.26E-05	1.12E-02	500
	120.15	4.13E+03	2.22E-05	1.13E-02	511
Experiment 5 (10-20 mesh)	0.00	1.46E+04	7.84E-05	0.00E+00	---
	0.25	1.30E+04	6.98E-05	1.67E-03	25
	1.00	1.14E+04	6.12E-05	3.40E-03	56
	4.00	8.13E+03	4.37E-05	6.92E-03	160
	8.00	7.72E+03	4.15E-05	7.36E-03	179
	24.00	5.84E+03	3.14E-05	9.39E-03	301
	48.00	5.11E+03	2.74E-05	1.02E-02	373
	75.32	4.91E+03	2.64E-05	1.04E-02	396
	120.00	4.66E+03	2.50E-05	1.07E-02	428
Experiment 6 (20-40 mesh)	0.00	1.37E+04	7.36E-05	0.00E+00	---
	0.25	1.20E+04	6.44E-05	1.84E-03	29
	1.00	1.01E+04	5.42E-05	3.90E-03	72
	4.00	7.43E+03	3.99E-05	6.79E-03	170
	8.00	6.43E+03	3.45E-05	7.87E-03	228
	24.00	4.79E+03	2.57E-05	9.65E-03	375
	48.05	4.31E+03	2.31E-05	1.02E-02	439
	74.45	4.25E+03	2.28E-05	1.02E-02	448
	120.00	4.20E+03	2.26E-05	1.03E-02	456
Experiment 7 (40-60 mesh)	0.00	1.37E+04	7.36E-05	0.00E+00	---
	0.27	1.11E+04	5.96E-05	2.85E-03	48
	1.00	8.99E+03	4.83E-05	5.15E-03	107
	4.00	6.39E+03	3.43E-05	8.00E-03	233
	8.00	5.39E+03	2.89E-05	9.09E-03	314
	24.00	4.41E+03	2.37E-05	1.02E-02	429
	48.05	4.09E+03	2.20E-05	1.05E-02	479
	74.48	4.19E+03	2.25E-05	1.04E-02	462
	120.08	4.04E+03	2.17E-05	1.06E-02	487

Table 4-5. Experimental variables for flow rate dependent kinetics testing.

Variable		Experiment 2	Experiment 8	Experiment 9
Start Date		08/27/02	10/04/02	10/12/02
Simulant		AN-105	AN-105	AN-105
Avg. Temperature (°C)		24.7	25.2	25.2
Sieve Fraction		Unsieved	Unsieved	Unsieved
Resin Dry Wt. (g)		0.5834	0.5801	0.5788
Feed Volume (mL)		120	120	120
Phase Ratio (ϕ)		206	207	207
c_i (Re)	**(µg/L)**	1.44E+04	1.45E+04	1.47E+04
	(M)	7.73E-05	7.79E-05	7.89E-05
Flow Rate	**(mL/min)**	30	1	0.5
	(BV/hr)	1385	46	23
	(cm/min)	12.5	0.416	0.208

Table 4-6. Results summary for flow rate dependent kinetics testing.

Experiment (Flow rate)	Time, t (hr)	Liquid Re Concentration (c_f)		Loading, Q (mmol Re/g resin)	K_d (mL/g)
		(μg/L)	(M)		
Experiment 2 (30 mL/min, 12.5 cm/min)	0.00	1.44E+04	7.73E-05	0.00E+00	---
	0.25	1.19E+04	6.39E-05	2.71E-03	43
	1.00	9.58E+03	5.14E-05	5.27E-03	103
	4.02	7.35E+03	3.95E-05	7.73E-03	197
	8.00	6.25E+03	3.36E-05	8.95E-03	268
	24.48	4.84E+03	2.60E-05	1.05E-02	406
	49.62	4.32E+03	2.32E-05	1.11E-02	480
	72.23	4.20E+03	2.26E-05	1.12E-02	500
	120.15	4.13E+03	2.22E-05	1.13E-02	511
Experiment 8 (1 mL/min, 0.416 cm/min)	0.00	1.45E+04	7.79E-05	0.00E+00	---
	0.25	1.33E+04	7.14E-05	1.33E-03	19
	1.00	1.14E+04	6.12E-05	3.44E-03	56
	4.00	8.38E+03	4.50E-05	6.80E-03	151
	8.02	7.13E+03	3.83E-05	8.19E-03	214
	24.00	4.98E+03	2.67E-05	1.06E-02	395
	48.00	4.48E+03	2.41E-05	1.11E-02	463
	72.00	4.31E+03	2.31E-05	1.13E-02	489
	120.00	4.23E+03	2.27E-05	1.14E-02	502
Experiment 9 (0.5 mL/min, 0.208 cm/min)	0.00	1.47E+04	7.89E-05	0.00E+00	---
	0.25	1.40E+04	7.52E-05	7.24E-04	10
	1.00	1.38E+04	7.41E-05	9.46E-04	14
	4.00	1.37E+04	7.36E-05	1.06E-03	15
	8.00	1.13E+04	6.07E-05	3.73E-03	62
	24.00	6.65E+03	3.57E-05	8.91E-03	251
	48.03	5.15E+03	2.77E-05	1.06E-02	384
	72.00	4.67E+03	2.51E-05	1.11E-02	445
	120.00	4.39E+03	2.36E-05	1.14E-02	487

Table 4-7. Experimental variables for simulant dependent kinetics testing.

Variable		Experiment 2	Experiment 10	Experiment 11
Start Date		08/27/02	09/26/02	09/26/02
Simulant		AN-105	AZ-102	AN-107
Avg. Temperature (°C)		24.7	24.7	24.7
Sieve Fraction		Unsieved	Unsieved	Unsieved
Resin Dry Wt. (g)		0.5834	0.5932	0.5932
Feed Volume (mL)		120	120	120
Phase Ratio (ϕ)		206	202	202
c_i (Re)	**(μg/L)**	1.44E+04	3.96E+04	6.66E+04
	(M)	7.73E-05	2.13E-04	3.58E-05
Flow Rate	**(mL/min)**	30	30	30
	(BV/hr)	1385	1385	1385
	(cm/min)	12.5	12.5	12.5

Table 4-8. Results summary for simulant dependent kinetics testing.

Experiment (Simulant)	Time, t (hr)	Liquid Re Concentration (c_f)		Loading, Q (mmol Re/g resin)	K_d (mL/g)
		(μg/L)	(M)		
Experiment 2 (AN-105)	0.00	1.44E+04	7.73E-05	0.00E+00	---
	0.25	1.19E+04	6.39E-05	2.71E-03	43
	1.00	9.58E+03	5.14E-05	5.27E-03	103
	4.02	7.35E+03	3.95E-05	7.73E-03	197
	8.00	6.25E+03	3.36E-05	8.95E-03	268
	24.48	4.84E+03	2.60E-05	1.05E-02	406
	49.62	4.32E+03	2.32E-05	1.11E-02	480
	72.23	4.20E+03	2.26E-05	1.12E-02	500
	120.15	4.13E+03	2.22E-05	1.13E-02	511
Experiment 10 (AZ-102)	0.00	3.96E+04	2.13E-04	0.00E+00	---
	0.25	2.87E+04	1.54E-04	1.18E-02	77
	0.98	2.22E+04	1.19E-04	1.88E-02	159
	4.05	1.35E+04	7.25E-05	2.83E-02	391
	8.00	1.12E+04	6.01E-05	3.08E-02	513
	23.97	8.44E+03	4.53E-05	3.38E-02	747
	47.73	7.71E+03	4.14E-05	3.46E-02	837
	71.58	6.44E+03	3.46E-05	3.60E-02	1042
	120.00	6.51E+03	3.50E-05	3.59E-02	1028
Experiment 11 (AN-107)	0.00	6.66E+03	3.58E-05	0.00E+00	---
	0.28	4.97E+03	2.67E-05	1.84E-03	69
	1	4.46E+03	2.40E-05	2.39E-03	100
	4.07	3.55E+03	1.91E-05	3.38E-03	177
	8.02	3.34E+03	1.79E-05	3.61E-03	201
	24.02	2.88E+03	1.55E-05	4.11E-03	266
	47.77	2.83E+03	1.52E-05	4.16E-03	274
	71.6	2.90E+03	1.56E-05	4.08E-03	262
	120.02	3.03E+03	1.63E-05	3.94E-03	242
Experiment 11 (AN-107) (ICP-ES)	0.00	5.85E+03	3.14E-05	0.00E+00	---
	0.28	5.00E+03	2.69E-05	9.23E-04	34
	1.00	4.40E+03	2.36E-05	1.58E-03	67
	4.07	3.50E+03	1.88E-05	2.55E-03	136
	8.02	3.20E+03	1.72E-05	2.88E-03	168
	24.02	2.80E+03	1.50E-05	3.31E-03	220
	47.77	2.40E+03	1.29E-05	3.75E-03	291
	71.60	2.70E+03	1.45E-05	3.42E-03	236
	120.02	2.70E+03	1.45E-05	3.42E-03	236

Table 4-9. Approximate molar concentration levels and molar ratios for the key ions contained in the Envelope A, B, and C simulants examined.

Key Ion Variables	Envelope A (AN-105)	Envelope B (AZ-102)	Envelope C (AN-107)
$[Na^+]$	4.91	4.67	5.74
$[K^+]$	0.10	0.15	0.04
$[NO_3^-]$	1.243	0.515	2.625
$[ReO_4^-]$	6.270E-05	1.880E-04	3.222E-05
$[NO_3^-] / [ReO_4^-]$	19800	2740	81500
$[Na^+] / [K^+]$	12.4	3.4	65.6
$[Na^+] + [K^+]$	5.01	4.82	5.78

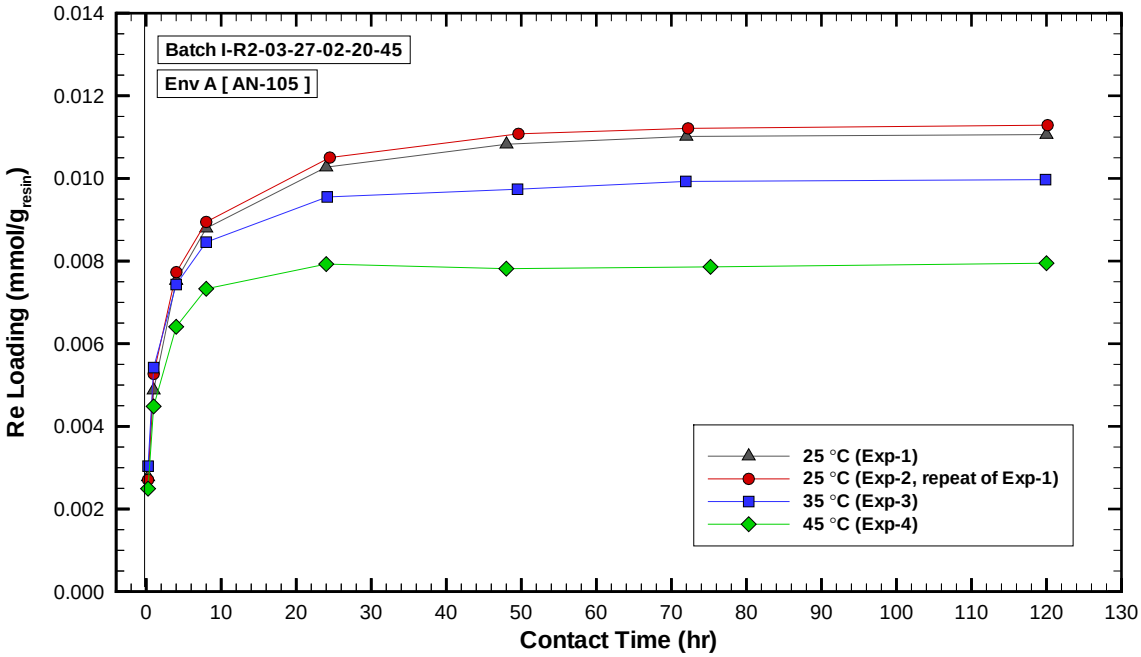

Figure 4-1. Transient Re loading levels for various contact temperatures. Exp-1 and Exp-2 demonstrate the level of reproducibility at 25 ºC.

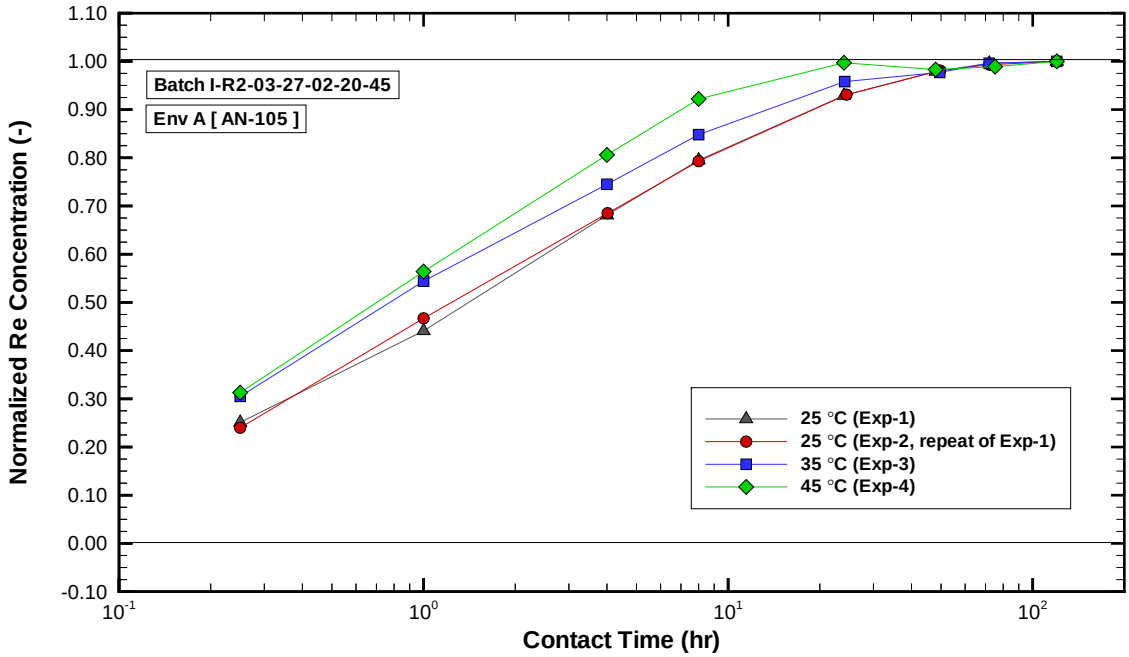

Figure 4-2. Transient normalized Re concentration levels for various contact temperatures. Exp-1 and Exp-2 demonstrate the level of reproducibility at 25 ºC.

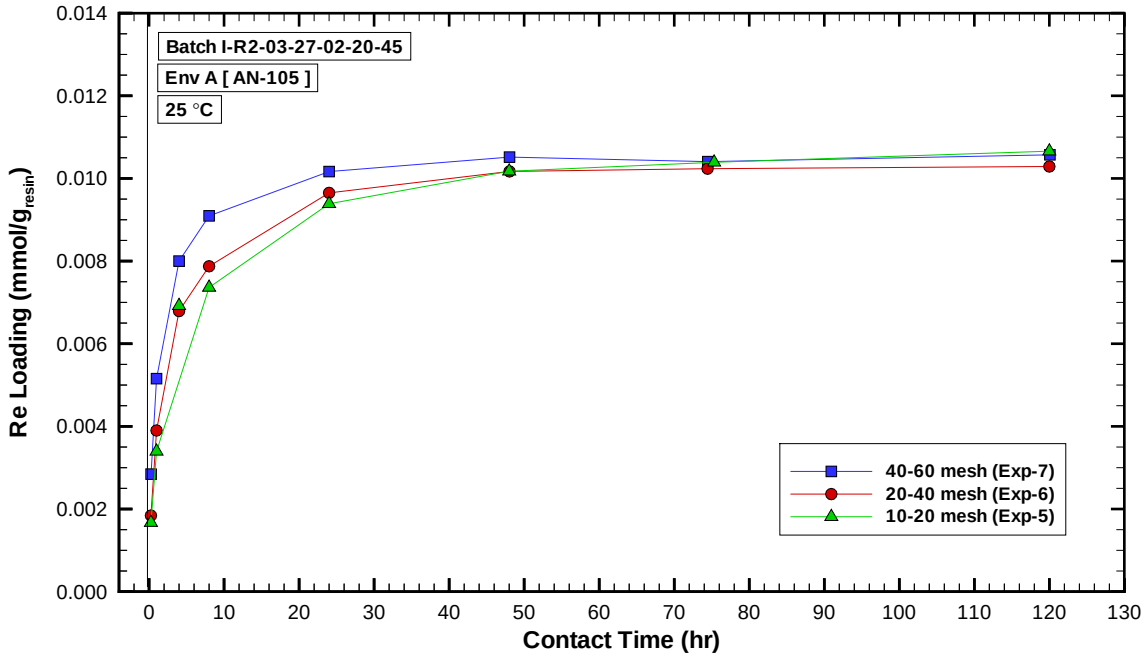

Figure 4-3. Transient Re loading levels for the various sieve fractions.

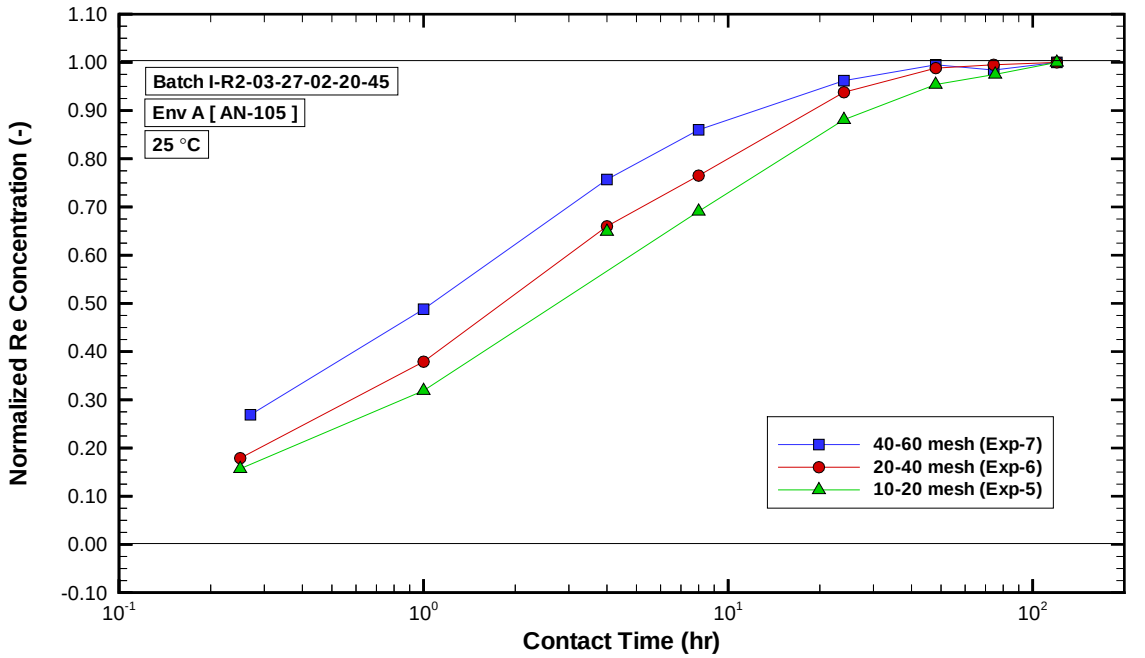

Figure 4-4. Transient normalized Re concentration levels for the various sieve fractions.

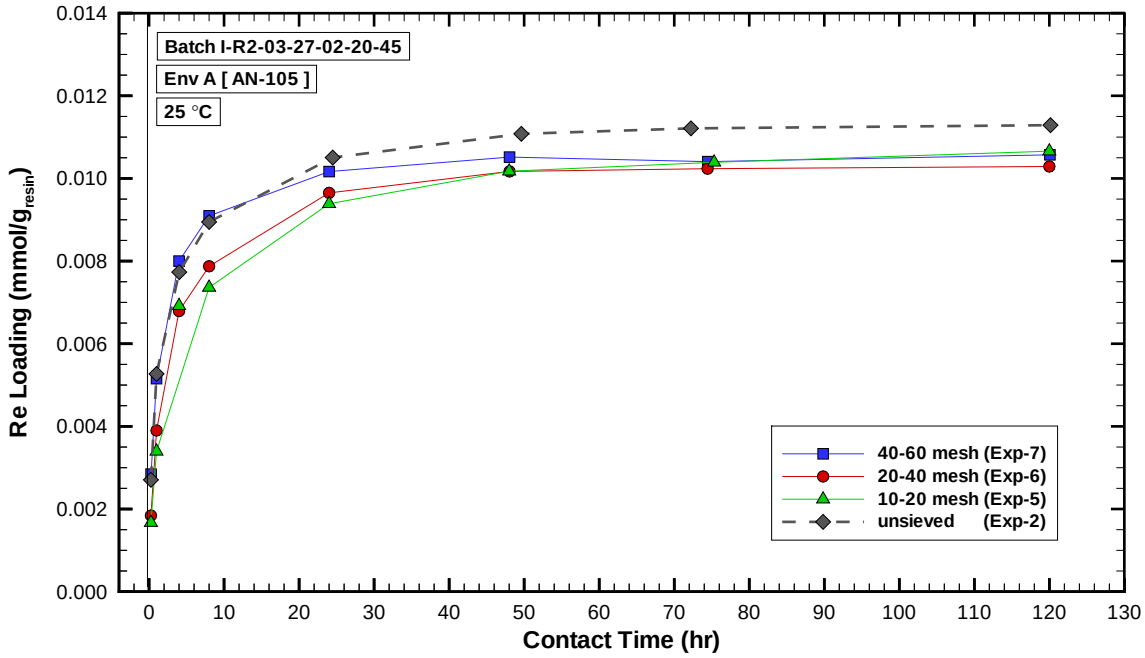

Figure 4-5. Comparison of transient Re loading levels for the various sieve fractions versus the unsieved composite.

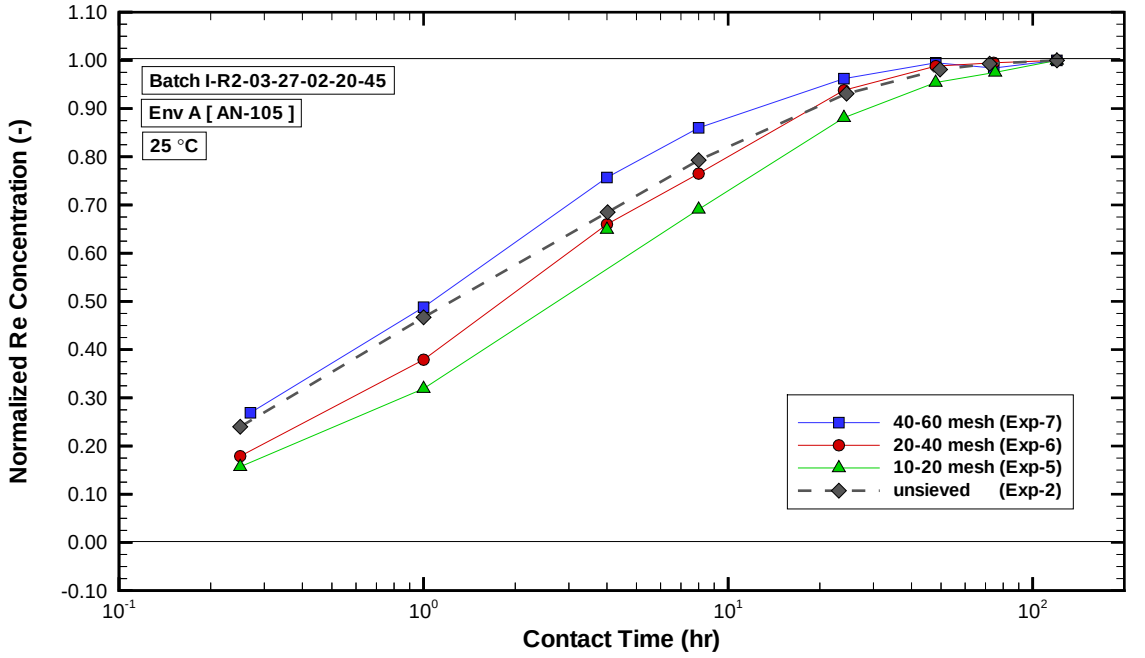

Figure 4-6. Comparison of transient normalized Re concentration levels for the various sieve fractions versus the unsieved composite.

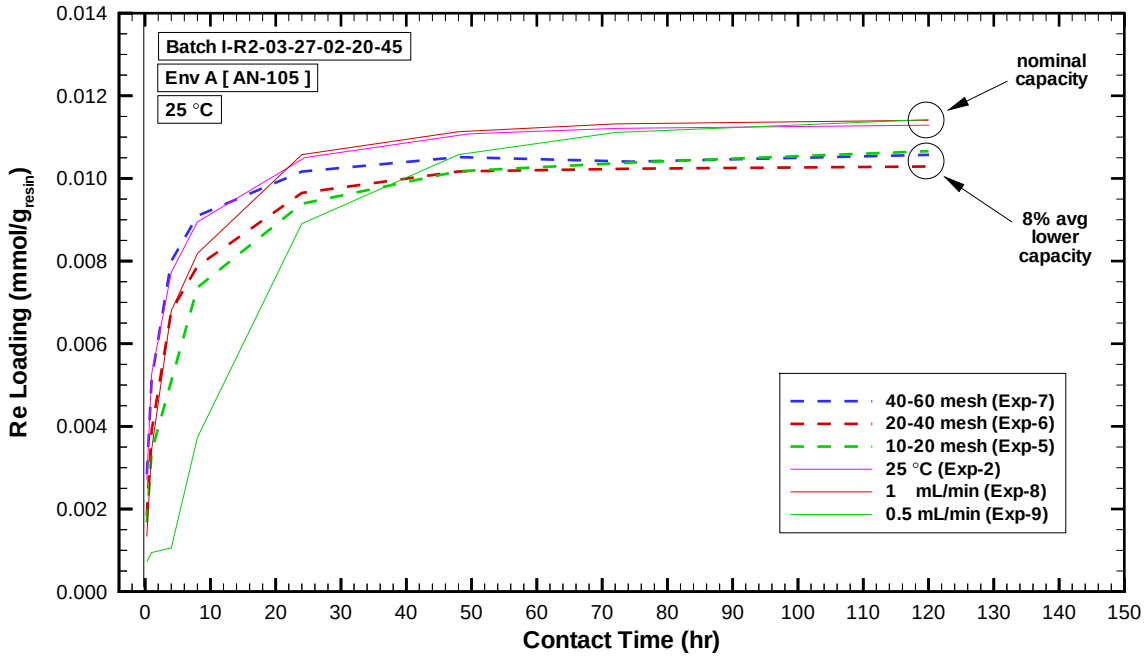

Figure 4-7. Comparison of transient Re loading levels for all the kinetics experiments performed at 25ºC and with AN-105 simulant. An approximately 8% reduction in measured Re loading is observed for sieved versus unsieved resin samples.

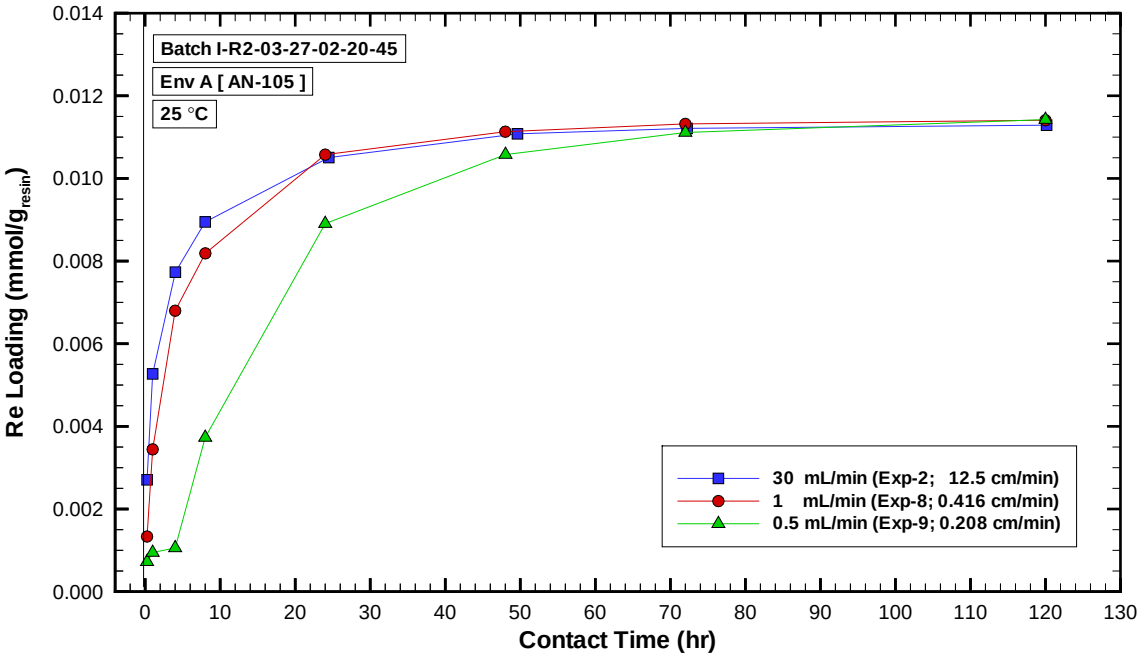

Figure 4-8. Comparison of transient Re loading levels at the various flow rates.

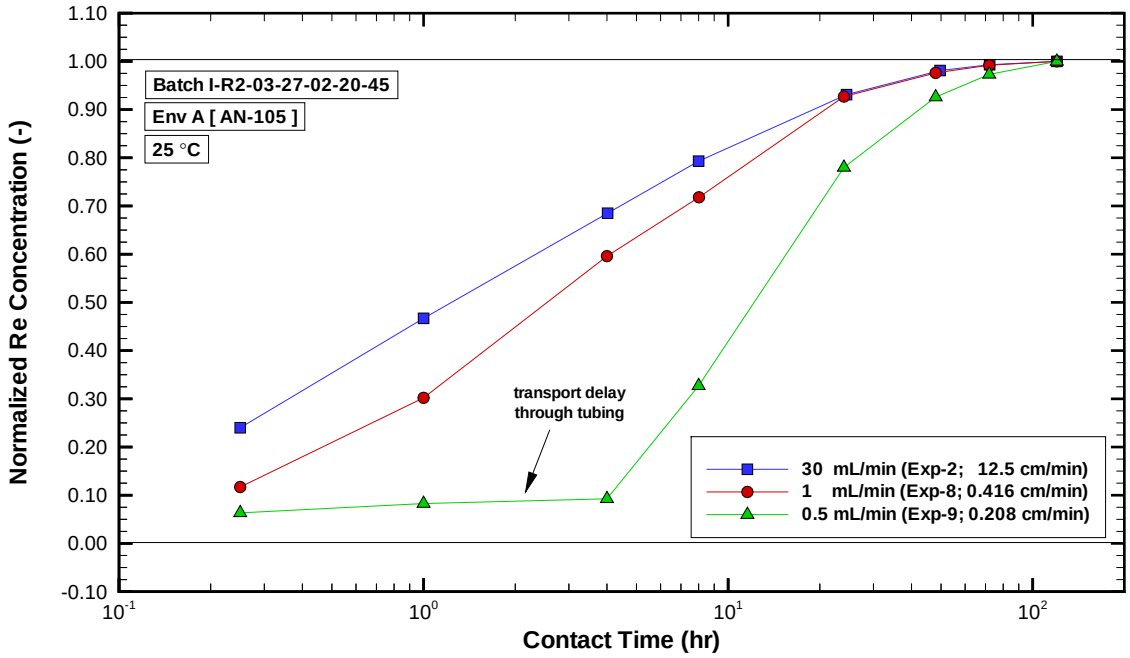

Figure 4-9. Comparison of transient normalized Re concentration levels at the various flow rates.

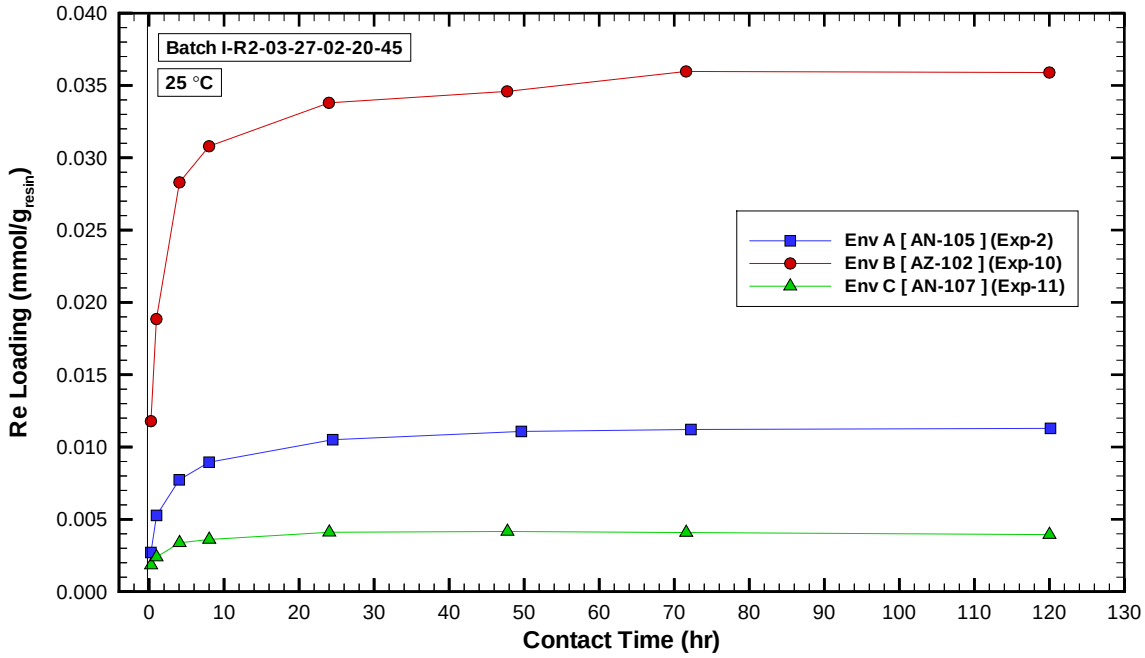

Figure 4-10. Transient Re loading levels for Envelope A, B, and C simulants.

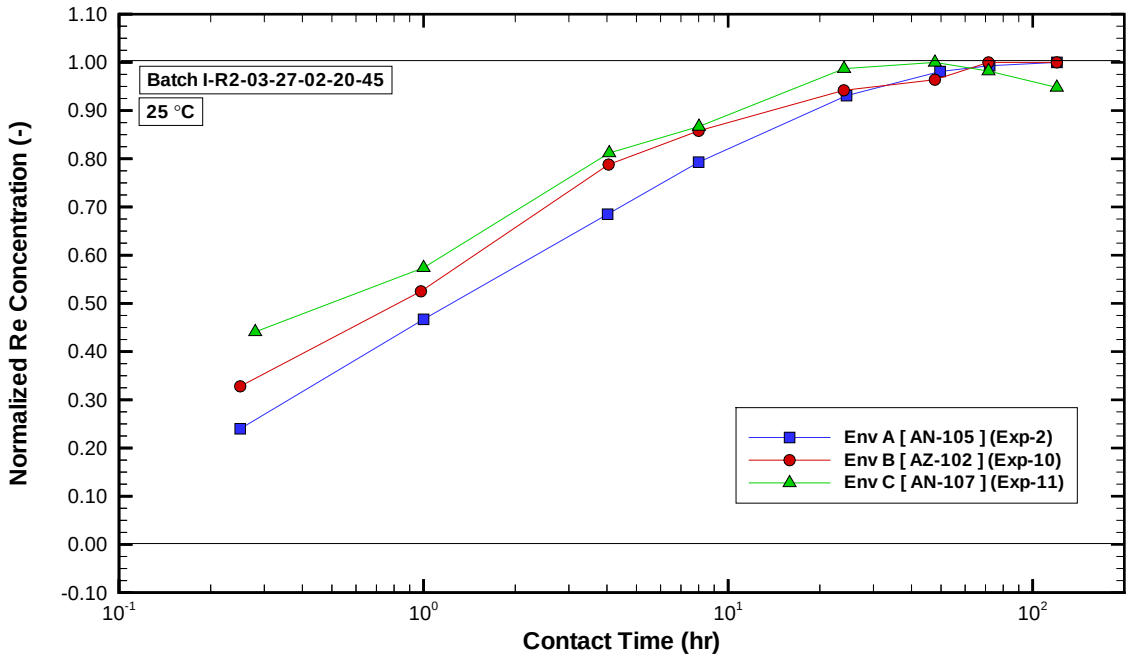

Figure 4-11. Transient normalized Re concentration levels for Envelope A, B, and C simulants.

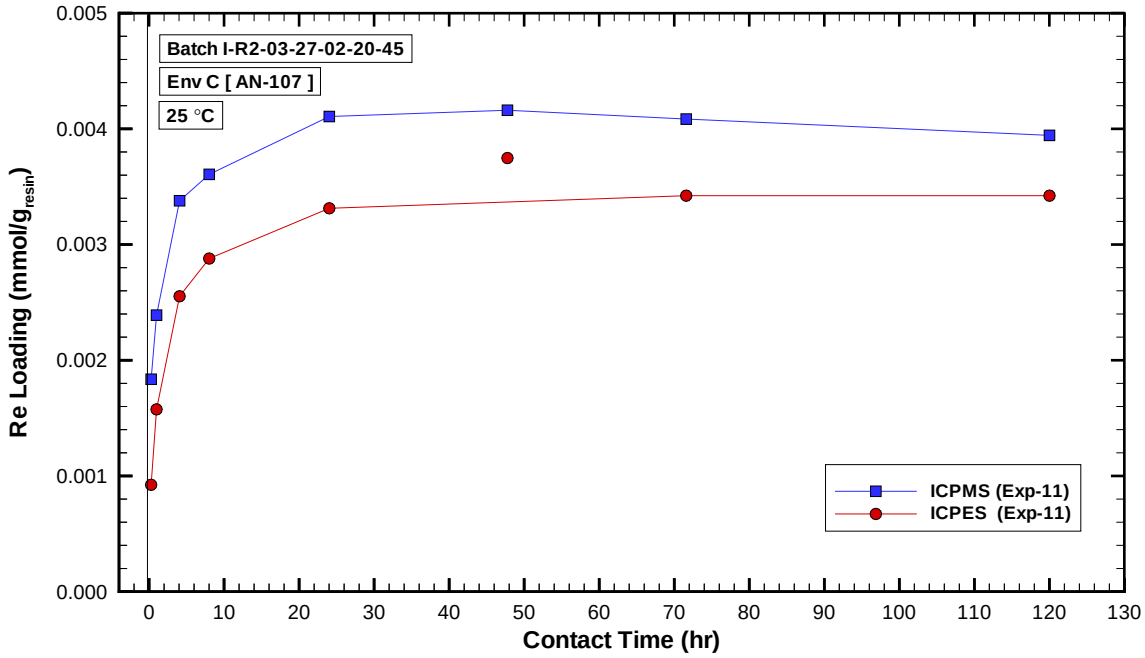

Figure 4-12. Transient Re loading levels for Envelope C simulant based on ICPMS and ICPES measurement techniques.

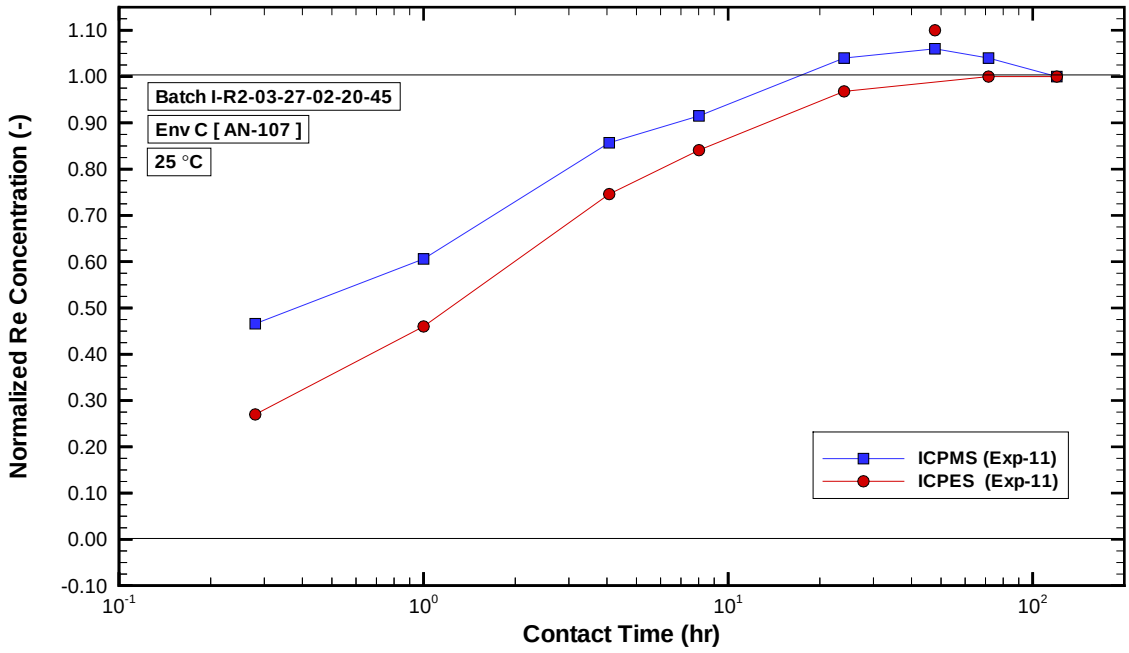

Figure 4-13. Transient normalized Re concentration levels for Envelope C simulant based on ICP-MS and ICP-ES measurement techniques.

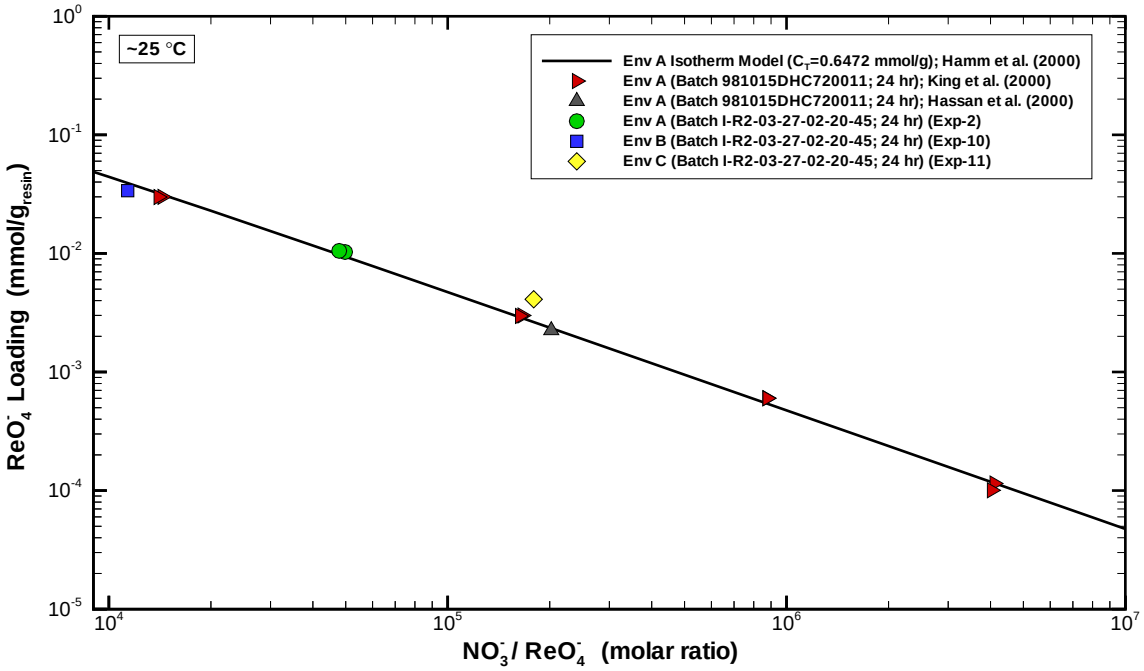

Figure 4-14. Comparison of perrhenate loading data versus major competitor (nitrate) for two different SuperLig® 639 batches in contact with Envelope A, B, and C simulants. The 25ºC algebraic isotherm model for batch 981015DHC720011 and AN-105 is shown.

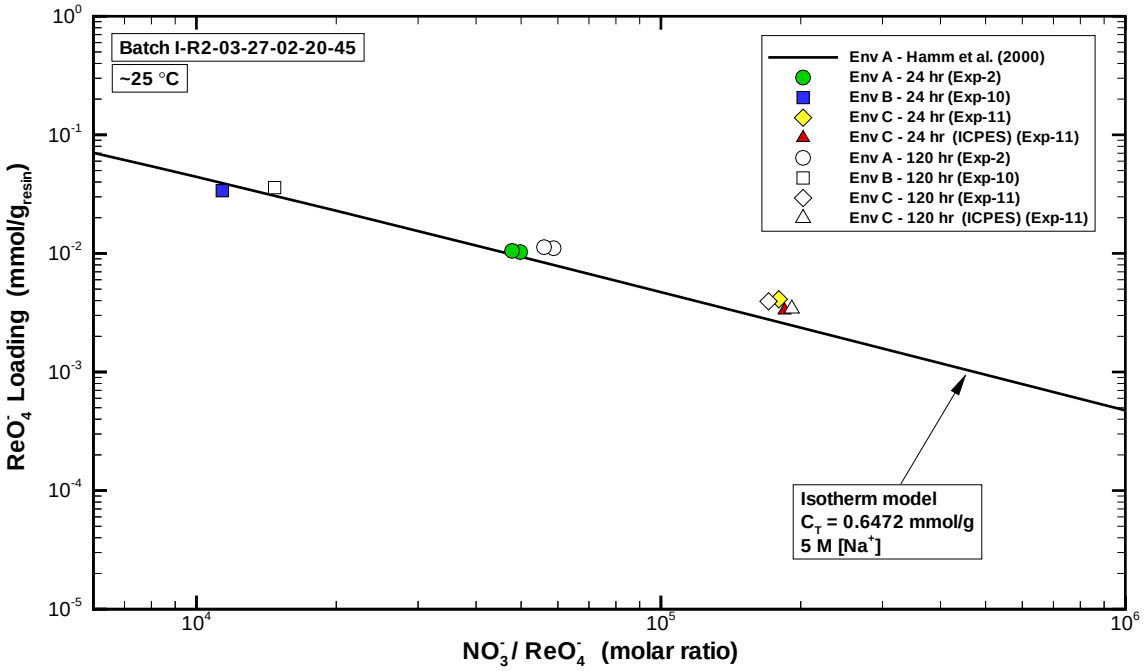

Figure 4-15. Comparison of perrhenate loading data versus major competitor (nitrate) for SuperLig® 639 with 24- and 120-hr contact times, Envelope A, B, and C simulants (ICP-ES shown in addition to ICP-MS for Envelope C), and algebraic isotherm model.

5.0 Conclusions

- Temperature dependent testing was performed at 25, 35, and 45°C using unsieved SuperLig®639 resin and standard Envelope A (AN-105) simulant. As expected, the adsorption capacity of the resin drops at higher temperatures. A drop in capacity of approximately 1.5% is observed for every 1°C increase in contact temperature. In addition, particle kinetics were faster at higher temperatures which was also expected. No resin degradation or slower competitor effects were observed over the 120-hour contact period.

- Particle size dependent testing was performed using three sieve fractions (10-20 mesh, 20-40 mesh, and 40-60 mesh) of SuperLig®639 resin and standard Envelope A (AN-105) simulant. As expected, the adsorption capacity of the resin was independent of particle size. In addition, particle kinetics were faster for the smaller particles which was also expected. No resin degradation or slower competitor effects were observed over the 120-hour contact period.

- Flow rate dependent testing was performed using unsieved SuperLig®639 resin, standard Envelope A (AN-105) simulant, and flow rates of 0.5 mL/min (0.208 cm/min), 1 mL/min (0.416 cm/min), as well as the nominal flow rate of 30 mL/min (12.5 cm/min). As expected, the adsorption capacity of the resin was independent of the flow rate. No resin degradation or slower competitor effects were observed over the 120-hour contact period.

- Simulant dependent testing was performed using unsieved SuperLig®639 resin and Envelope A (AN-105), Envelope B (AZ-102), and Envelope C (AN-107) simulants. As expected, the adsorption capacity of the resin varied inversely with the nitrate-to-perrhenate ratio. No resin degradation or slower competitor effects were observed over the 120-hour contact period.

- The adsorption capacity resulting from testing performed using unsieved SuperLig®639 resin and Envelope A (AN-105) simulant at 25°C was quite reproducible. This indicates that the kinetics test apparatus and methodology provides an excellent means of determining particle kinetics as well as the true equilibrium state.

6.0 References

Dobos, J., 2002. "Chromatographic Resin Support", U.S. Patent #6,440,301,B1. Submitted by Westinghouse Savannah River Company.

Eibling, R. E., C. A. Nash, 2001. "Hanford Waste Simulants Created to Support the Research and Development on the River Protection Project – Waste Treatment Plant", Westinghouse Savannah River Company document,WSRC-TR-2000-00338 (SRT-RPP-2000-00017), Rev. 0, February.

Froment, G. F. and K. B. Bishoff, 1979. Chemical Reactor Analysis and Design, John Wiley and Sons, Inc., New York.

Hamm, L. L., F. G. Smith, III, and D. J. McCabe, 2000a. "Preliminary Ion-exchange Modeling for Removal of Cesium from Hanford Waste Using SuperLig® 644 Resin," BNF-003-98-0220, June 16.

Hamm, L. L., F. G. Smith, III, and D. J. McCabe, 2000b. "Preliminary Ion-exchange Modeling for Removal of Technetium from Hanford Waste Using SuperLig® 639 Resin," WSRC-TR-2000-00305 (SRT-RPP-2000-00011), August.

Hamm, L. L., T. Hang, D. J. McCabe, and W. D. King, 2002. "Preliminary Ion-exchange Modeling for Removal of Cesium from Hanford Waste Using Hydrous Crystalline Silicotitanate Material," WSRC-TR-2001-00400 (SRT-RPP-2001-00134), December.

Hassan, N. M., D. J. McCabe, and W. D. King, 2000. "Small-Scale Ion-exchange Removal of Cesium and Technetium from Hanford Tank 241-AN-103," BNF-003-98-0146, Revision 1, April 12.

Johnson, M. E., 2001. "Test Specification: Evaluating Effects of Resin Particle Size and Solution Temperature on SuperLig® 644 and SuperLig®- 639 Resins Performance with LAW Envelope A Simulant," Bechtel Hanford document, TSP-W375-01-00023, Rev. 0 (February).

King, W. D., D. J. McCabe, and N. M. Hassan, 2000. "Evaluation of SuperLig 639 Ion-exchange Resin for the Removal of Rhenium from Hanford Envelope A Simulant," Westinghouse Savannah River Company document, BNF-003-98-0230, Rev. 0, April 13.

King, W. D., W. A. Spencer, and M. P. Bussey, 2003. "Laboratory-Scale SuperLig® 639 Column Tests with Hanford Waste Simulants (U)," Westinghouse Savannah River Company document, WSRC-TR-2002-00580 (SRT-RPP-2002-00266), Rev. 0, January.

McCabe, D. J., 2001. "Task Technical and Quality Assurance Plan Evaluating Effects of Resin Particle Size and Solution Temperature on SuperLig® 644 and SuperLig®- 639 Resins Performance with LAW Envelope A Simulant (U)," Westinghouse Savannah River Co. document, WSRC-TR-2001-00202 (SRT-RPP-2001-00049), Rev. 0 (July 13).

Smith, J. M., 1981. Chemical Engineering Kinetics, 3rd ed., McGraw Hill, New York, pp. 331-332.

Steimke, J. L., M. A. Norato, T. J. Steeper, and D. J. McCabe, 2000. "Summary of Testing of SuperLig® 639 at the TFL Ion-exchange Facility," WSRC-TR-2000-00302 (SRT-RPP-2000-00008), Rev. 0, August 24.

Sundar, P. S., 2002. "Test Exception for Test Specification: Evaluating Effects of Resin Particle Size and Solution Temperature on SuperLig® 644 and SuperLig®- 639 Resins Performance with LAW Envelope A Simulant (Johnson, 2001)," Bechtel Hanford document, 24590-WTP-TEF-RT-02-010, Rev. 1 (October 24).

Whitley, R. D. and L. N.-H. Wang, 1996. "User's Manual VERSE (VErsatile Reaction SEparation) Simulation for Liquid Phase Adsorption and Chromatography Processes," Purdue University.

Wilson, E. J. and C. J. Geankoplis, 1966. "Liquid Mass Transfer at Very Low Reynolds Numbers in Packed Beds," Industrial and Engineering Chemistry Fundamentals, Vol. 5, No. 1, pp. 9-14.

(This Page Intentionally Left Blank)

Appendix A. Analytical Results for Experiment 1

Table A-1. ICP-ES data for Experiment 1

Species	Feed 1 (mg/L)	Feed 2 (mg/L)	120 h (mg/L)
Al	15800	15900	15400
B	24.8	24.4	24.4
Ba	0.18	0.16	0.26
Ca	<0.2	0.26	0.40
Cd	1.22	1.21	1.14
Co	<0.22	<0.22	<0.22
Cr	616	617	591
Cu	<0.25	<0.25	<0.4
Fe	4.21	4.10	4.73
Li	<0.5	<0.5	<0.5
Mg	<0.42	<0.42	<0.42
Mn	<0.045	<0.045	<0.045
Mo	38.0	37.5	36.6
Na	114000	119000	112000
Ni	<0.31	<0.31	<0.31
P	75.8	73.3	74.0
Pb	23.9	23.6	23.3
Si	101	99.4	102
Sn	<1.3	<1.3	<1.3
Sr	0.019	0.010	0.061
Ti	<0.7	<0.7	<0.7
V	<0.65	<0.65	<0.65
Zn	4.45	4.34	4.44
Zr	<0.24	0.31	0.29
Nb	<2.5	<2.5	<2.5
La	<3.5	<3.5	<3.5
K	3680	3710	3490
Re	14.0	13.8	4.22
S	128	124	125

Table A-2. IC Anion data for Experiment 1

Anion	Feed (μg/mL)	120 h (μg/mL)
Fluoride	<20	<20
Formate	1620	1570
Chloride	4150	4020
Nitrite	53300	51800
Nitrate	70000	66800
Phosphate	244	239
Sulfate	318	304
Oxalate	148	149

Appendix B. Analytical Results for Experiment 2

Table B-1. ICP-ES data for Experiment 2

Species	Feed 1 (mg/L)	Feed 2 (mg/L)	120 h (mg/L)
Al	16000	16000	15600
B	26.5	26.3	27.0
Ba	0.21	0.17	0.28
Ca	<0.4	<0.4	<0.4
Cd	1.53	1.63	1.34
Co	<0.44	<0.44	<0.44
Cr	630	631	612
Cu	<0.5	<0.5	<0.5
Fe	4.01	4.23	4.64
Li	<1	<1	<1
Mg	<0.84	<0.84	<0.84
Mn	<0.09	<0.09	<0.09
Mo	38.0	38.6	37.9
Na	107000	104000	107000
Ni	<0.62	<0.62	<0.62
P	80.1	79.1	75.5
Pb	22.3	23.1	22.9
Si	95.0	95.2	105
Sn	<2.6	<2.6	<2.6
Sr	<0.05	<0.05	<0.05
Ti	<1.4	<1.4	<1.4
V	<1.3	<1.3	<1.3
Zn	5.09	5.11	5.05
Zr	<0.48	<0.48	<0.48
La	<7	<7	<7
K	3680	3670	3520
Re	14.6	14.4	4.43
S	127	123	127

Table B-2. IC Anion data for Experiment 2

Anion	Feed (μg/mL)	120 h (μg/mL)
Fluoride	<20	<20
Formate	1700	1690
Chloride	3910	3890
Nitrite	52000	51100
Nitrate	69500	70100
Phosphate	144	146
Sulfate	315	314
Oxalate	211	212

Appendix C. Analytical Results for Experiment 3

Table C-1. ICP-ES data for Experiment 3

Species	Feed 1 (mg/L)	Feed 2 (mg/L)	120 h (mg/L)
Al	16000	16000	15900
B	26.5	26.3	27.70
Ba	0.21	0.17	0.20
Ca	<0.4	<0.4	<0.4
Cd	1.53	1.63	1.38
Co	<0.44	<0.44	<0.44
Cr	630	631	630
Cu	<0.5	<0.5	<0.5
Fe	4.01	4.23	4.67
Li	<1	<1	<1
Mg	<0.84	<0.84	<0.84
Mn	<0.09	<0.09	<0.09
Mo	38.0	38.6	38.2
Na	107000	104000	104000
Ni	<0.62	<0.62	<0.62
P	80.1	79.1	80.2
Pb	22.3	23.1	23.0
Si	95.0	95.2	118
Sn	<2.6	<2.6	<2.6
Sr	<0.05	<0.05	<0.05
Ti	<1.4	<1.4	<1.4
V	<1.3	<1.3	<1.3
Zn	5.09	5.11	5.13
Zr	<0.48	<0.48	<0.48
La	<7	<7	<7
K	3680	3670	3690
Re	14.6	14.4	5.49
S	127	123	128

Table C-2. IC Anion data for Experiment 3

Anion	Feed (μg/mL)	120 h (μg/mL)
Fluoride	<20	<20
Formate	1700	1700
Chloride	3910	3910
Nitrite	52000	51600
Nitrate	69500	67900
Phosphate	144	142
Sulfate	315	317
Oxalate	211	204

Appendix D. Analytical Results for Experiment 4

Table D-1. ICP-ES data for Experiment 4

Species	Feed 1 (mg/L)	Feed 2 (mg/L)	120 h (mg/L)
Al	16400	16000	16200
B	22.3	23.6	32.4
Ba	<0.12	0.15	1.97
Ca	3.41	<0.4	<0.4
Cd	1.46	1.41	1.38
Co	<0.44	<0.44	<4.4
Cr	624	627	622
Cu	<0.5	<0.5	<0.5
Fe	3.87	3.96	5.65
Li	<1	<1	<1
Mg	<0.84	<0.84	<0.84
Mn	<0.09	<0.09	<0.09
Mo	37.6	37.5	37.2
Na	111000	115000	115000
Ni	<0.62	<0.62	<0.62
P	89.7	100	83.8
Pb	21.4	24.2	22.7
Si	95.1	95.3	119
Sn	<2.6	<2.6	<2.6
Sr	<0.05	<0.05	<0.040
Ti	<1.4	<1.4	<1.4
V	<1.3	<1.3	<1.3
Zn	5.09	5.13	5.28
Zr	<0.48	<0.48	<0.48
Nb	<5	<5	---
La	<7	<7	<7
K	3640	3680	3600
Re	14.2	14.8	7.1
S	124	130	126

Table D-2. IC Anion data for Experiment 4

Anion	Feed (μg/mL)	120 h (μg/mL)
Fluoride	<20	<20
Formate	1730	1770
Chloride	4050	4100
Nitrite	23800	53100
Nitrate	64700	63900
Phosphate	155	164
Sulfate	295	317
Oxalate	184	215

Appendix E. Analytical Results for Experiment 5

Table E-1. ICP-ES data for Experiment 5

Species	Feed 1 (mg/L)	Feed 2 (mg/L)	120 h (mg/L)
Al	16400	16000	15800
B	22.3	23.6	24.5
Ba	<0.12	0.15	0.32
Ca	3.41	<0.4	<0.4
Cd	1.46	1.41	1.29
Co	<0.44	<0.44	<0.44
Cr	624	627	606
Cu	<0.5	<0.5	<0.5
Fe	3.87	3.96	4.80
Li	<1	<1	<1
Mg	<0.84	<0.84	<0.84
Mn	<0.09	<0.09	0.18
Mo	37.6	37.5	35.8
Na	111000	115000	110000
Ni	<0.62	<0.62	<0.62
P	89.7	100	77.4
Pb	21.4	24.2	22.7
Si	95.1	95.3	119
Sn	<2.6	<2.6	<2.6
Sr	<0.05	<0.05	0.088
Ti	<1.4	<1.4	<1.4
V	<1.3	<1.3	<1.3
Zn	5.09	5.13	4.85
Zr	<0.48	<0.48	<0.48
Nb	<5	<5	---
La	<7	<7	<7
K	3640	3680	3540
Re	14.2	14.8	4.2
S	124	130	122

Table E-2. IC Anion data for Experiment 5

Anion	Feed (μg/mL)	120 h (μg/mL)
Fluoride	<20	<20
Formate	1730	1690
Chloride	4050	3910
Nitrite	23800	51800
Nitrate	64700	61100
Phosphate	155	147
Sulfate	295	288
Oxalate	184	174

Appendix F. Analytical Results for Experiment 6

Table F-1. ICP-ES data for Experiment 6

Species	Feed 1 (mg/L)	Feed 2 (mg/L)	120 h (mg/L)
Al	16200	16000	16100
B	28.3	32.7	26.0
Ba	1.87	2.02	1.66
Ca	<0.4	<0.4	<0.4
Cd	1.28	1.37	1.33
Co	<0.44	<0.44	<0.44
Cr	622	630	613
Cu	<0.25	<0.25	<0.25
Fe	5.19	5.73	4.93
Li	<1	<1	<1
Mg	<0.84	<0.84	<0.84
Mn	<0.09	<0.09	<0.09
Mo	38.8	39.5	38.0
Na	113000	116000	111000
Ni	<0.62	<0.62	<0.62
P	79.4	83.3	79.5
Pb	25.5	27.0	24.9
Si	129	121	122
Sn	<2.6	<2.6	<2.6
Sr	<0.080	<0.080	<0.080
Ti	<1.4	<1.4	<1.4
V	<1.3	<1.3	<1.3
Zn	5.1	6.2	4.9
Zr	<0.48	<0.48	<0.48
La	<7	<7	<7
K	3590	3620	3540
Re	7.8	7.9	8.0
S	127	130	127

Table F-2. IC Anion data for Experiment 6

Anion	Feed (μg/mL)	120 h (μg/mL)
Fluoride	<20	<20
Formate	1630	1600
Chloride	3810	3720
Nitrite	52300	5120
Nitrate	69600	64500
Phosphate	161	154
Sulfate	303	301
Oxalate	189	187

Appendix G. Analytical Results for Experiment 7

Table G-1. ICP-ES data for Experiment 7

Species	Feed 1 (mg/L)	Feed 2 (mg/L)	120 h (mg/L)
Al	16200	16000	16000
B	28.3	32.7	22.7
Ba	1.87	2.02	0.24
Ca	<0.4	<0.4	<0.4
Cd	1.28	1.37	1.23
Co	<0.44	<0.44	<0.44
Cr	622	630	609
Cu	<0.25	<0.25	<0.25
Fe	5.19	5.73	4.51
Li	<1	<1	<1
Mg	<0.84	<0.84	<0.84
Mn	<0.09	<0.09	<0.09
Mo	38.8	39.5	37.4
Na	113000	116000	111000
Ni	<0.62	<0.62	<0.62
P	79.4	83.3	77.6
Pb	25.5	27.0	25.0
Si	129	121	103
Sn	<2.6	<2.6	<2.6
Sr	<0.080	<0.080	<0.080
Ti	<1.4	<1.4	<1.4
V	<1.3	<1.3	<1.3
Zn	5.1	6.2	4.8
Zr	<0.48	<0.48	<0.48
La	<7	<7	<7
K	3590	3620	3500
Re	7.8	7.9	4.8
S	127	130	124

Table G-2. IC Anion data for Experiment 7

Anion	Feed (μg/mL)	120 h (μg/mL)
Fluoride	<20	<20
Formate	1630	1600
Chloride	3810	3741
Nitrite	52300	51500
Nitrate	69600	67400
Phosphate	161	149
Sulfate	303	297
Oxalate	189	185

Appendix H. Analytical Results for Experiment 8

Table H-1. ICP-ES data for Experiment 8

Species	Feed 1 (mg/L)	Feed 2 (mg/L)	120 h (mg/L)
Al	16300	16100	15900
B	38.5	36.1	38.1
Ba	0.16	0.13	0.21
Ca	<0.4	<0.4	<0.4
Cd	1.39	1.42	1.27
Co	<0.44	<0.44	<0.44
Cr	627	628	620
Cu	<0.5	<0.5	<0.5
Fe	3.72	3.71	3.97
Li	<1	<1	<1
Mg	<0.84	<0.84	<0.84
Mn	<0.09	<0.09	<0.09
Mo	39.9	39.7	38.0
Na	117000	118000	118000
Ni	<0.62	<0.62	<0.62
P	91.4	91.7	93.5
Pb	23.9	23.5	22.2
Si	97.6	95.9	103
Sn	<2.6	<2.6	<2.6
Sr	<0.040	<0.040	<0.040
Ti	<1.4	<1.4	<1.4
V	<1.3	<1.3	<1.3
Zn	5.0	5.0	5.2
Zr	<0.48	<0.48	<0.48
La	<7	<7	<7
K	3870	3920	3740
Re	14.3	14.4	4.18
S	132	129	130

Table H-2. IC Anion data for Experiment 8

Anion	Feed (μg/mL)	120 h (μg/mL)
Fluoride	56	62
Formate	1330	1230
Chloride	2640	3500
Nitrite	40800	46800
Nitrate	60000	69400
Phosphate	156	285
Sulfate	298	166
Oxalate	172	---

Appendix I. Analytical Results for Experiment 9

Table I-1. ICP-ES data for Experiment 9

Species	Feed 1 (mg/L)	Feed 2 (mg/L)	120 h (mg/L)
Al	16300	16600	15700
B	28.29	27.6	28.5
Ba	0.32	0.30	0.34
Ca	<0.4	<0.4	<0.4
Cd	1.28	1.38	1.20
Co	<0.44	<0.44	<0.44
Cr	643	648	619
Cu	<0.5	<0.5	<0.5
Fe	3.6	3.6	3.8
Li	<1	<1	<1
Mg	<0.84	<0.84	<0.84
Mn	<0.09	<0.09	<0.09
Mo	39.9	40.1	38.7
Na	122000	120000	116000
Ni	0.87	0.72	<0.62
P	86.3	89.2	84.7
Pb	23.7	24.4	24.4
Si	97.2	96.6	104
Sn	<2.6	<2.6	<2.6
Sr	0.083	0.079	0.088
Ti	<1.4	<1.4	<1.4
V	<1.3	<1.3	<1.3
Zn	5.14	5.19	5.26
Zr	<0.48	<0.48	<0.48
La	<7	<7	<7
K	3880	3810	3670
Re	15.0	14.9	4.75
S	135	139	131

Appendix J. Analytical Results for Experiment 10

Table J-1. ICP-ES data for Experiment 10

Species	Feed 1 (mg/L)	Feed 2 (mg/L)	120 h (mg/L)
Al	1310	1320	1250
B	8.3	8.3	7.8
Ba	0.31	0.28	0.38
Ca	67.0	66.9	65.5
Cd	<0.14	<0.14	<0.14
Co	<0.44	<0.44	<0.44
Cr	1360	1370	1300
Cu	<0.25	<0.25	<0.25
Fe	<0.50	<0.50	14.5
Li	<1	<1	<1
Mg	<0.84	<0.84	<0.84
Mn	<0.09	<0.09	<0.09
Mo	106	106	101
Na	113000	114000	108000
Ni	<0.62	<0.62	<0.62
P	296	297	282
Pb	<6.9	<6.9	<6.9
Si	<1.3	<1.3	8.0
Sn	<2.6	<2.6	<2.6
Sr	0.59	0.59	0.53
Ti	<1.4	<1.4	<1.4
V	<1.3	<1.3	<1.3
Zn	<3.7	<3.7	<3.7
Zr	<0.48	<0.48	<0.48
La	<7	<7	<7
K	5860	5860	5520
Re	37.1	37.5	6.6
S	10200	10300	9650

Table J-2. IC Anion data for Experiment 10

Anion	Feed (μg/mL)	120 h (μg/mL)
Fluoride	2530	2380
Formate	7850	7630
Chloride	<20	<20
Nitrite	52300	50800
Nitrate	27400	26600
Phosphate	1030	1010
Sulfate	26500	25800
Oxalate	1420	1370

Appendix K. Analytical Results for Experiment 11

Table K-1. ICP-ES data for Experiment 11

Species	Feed 1 (mg/L)	Feed 2 (mg/L)	0.25 h (mg/L)	1 h (mg/L)	4 h (mg/L)	8 h (mg/L)	24 h (mg/L)	48 h (mg/L)	72 h (mg/L)	120 h (mg/L)
Al	246	253	244	247	252	237	244	246	254	252
B	22.2	22.4	20.8	21.1	21.4	20.8	21.4	22.0	22.3	22.9
Ba	<0.12	<0.12	<0.12	<0.12	<0.12	0.12	0.14	0.20	0.19	0.25
Ca	141	141	135	137	136	135	139	142	142	141
Cd	<0.20	<0.20	<0.20	<0.20	<0.20	<0.20	<0.20	<0.20	<0.20	<0.20
Co	<0.44	<0.44	<0.44	<0.44	<0.44	<0.44	<0.44	<0.44	<0.44	<0.44
Cr	<0.5	<0.5	<0.5	<0.5	<0.5	<0.5	0.60	0.50	0.55	0.56
Cu	<0.25	<0.25	<0.25	<0.25	<0.25	<0.25	<0.25	<0.25	<0.25	<0.25
Fe	17.1	17.2	16.7	16.6	16.7	16.1	16.5	16.7	16.9	17.0
Li	<1	<1	<1	<1	<1	<1	<1	<1	<1	<1
Mg	<0.84	<0.84	<0.84	<0.84	<0.84	<0.84	<0.84	<0.84	<0.84	<0.84
Mn	0.55	0.54	0.54	0.55	0.57	0.52	0.52	0.55	0.54	0.56
Mo	22.0	22.1	21.6	21.5	21.5	20.8	21.2	21.5	21.6	22.0
Na	129000	129000	124000	124000	125000	120000	123000	124000	127000	126000
Ni	319	317	306	308	311	301	309	311	315	313
P	304	303	295	293	294	283	290	294	296	299
Pb	<6.9	<6.9	<6.9	<6.9	<6.9	<6.9	<6.9	<6.9	<6.9	<6.9
Si	11.7	11.3	19.0	21.8	17.0	21.4	21.2	54.8	34.3	31.0
Sn	<2.6	<2.6	<2.6	<2.6	<2.6	<2.6	<2.6	<2.6	<2.6	<2.6
Sr	88.3	88.4	84.7	85.8	84.9	83.7	85.9	87.4	87.4	86.4
Ti	<1.4	<1.4	<1.4	<1.4	<1.4	<1.4	<1.4	<1.4	<1.4	<1.4
V	<1.3	<1.3	<1.3	<1.3	<1.3	<1.3	<1.3	<1.3	<1.3	<1.3
Zn	20.0	20.1	19.6	19.4	19.6	18.8	19.3	19.5	19.8	19.8
Zr	0.50	0.65	0.96	0.74	<0.48	0.81	0.83	<0.48	0.95	0.64
La	<7	<7	<7	<7	<7	<7	<7	<7	<7	<7
K	1390	1390	1310	1300	1290	1280	1310	1330	1330	1340
Re	5.9	5.8	5.0	4.4	3.5	3.2	2.8	2.4	2.7	2.7
S	1740	1750	1700	1700	1690	1630	1670	1700	1710	1720

Table K-2. IC Anion data for Experiment 11

Anion	Feed (μg/mL)	120 h (μg/mL)
Fluoride	1670	1679
Formate	5900	6320
Chloride	1240	1230
Nitrite	35900	36800
Nitrate	137000	135000
Phosphate	1610	1640
Sulfate	4670	4630
Oxalate	1080	1220